

Fundamental Bounds and Efficient Estimation for Dead-Time-Constrained Event Detection, with Application to Single-Photon Lidar

Frederic J. N. Jorgensen and Steven G. Johnson

Abstract—We develop an asymptotic statistical theory for parameter estimation from a class of non-i.i.d. periodic binary event-detection processes subject to nonparalyzable dead time and gating, which we call “dead-time event detection” (DED) processes. Such processes arise in single-photon lidar, fluorescence lifetime imaging, X-ray astronomy, and particle or radiation flux measurements in nuclear physics, where each detection renders the radiation/particle detector inactive for a recovery interval. Our theory quantifies how dead time and gating affect the fundamental lower bounds of estimation and identifies practical estimators that attain these bounds. First, we identify a sufficient statistic, showing in particular that activation counts can carry statistically useful information discarded by conventional histogramming hardware. We then prove local asymptotic normality and derive the corresponding Fisher-information rate, thereby obtaining fundamental lower bounds for estimation from DED processes. We prove that the maximum likelihood estimator (MLE), widely used in DED applications, attains these lower bounds. Since computing the MLE typically requires solving a nonconvex optimization problem, we also propose Le Cam one-step estimators, which attain the same asymptotic bounds with only a single local correction rather than iterative optimization. We illustrate the validity of our asymptotic theory and the practical usefulness of one-step estimators through the example of single-photon lidar in both simulations and real-data experiments.

Index Terms—Dead time, refractory time, Fisher information, asymptotic efficiency, single-photon lidar.

I. INTRODUCTION

We develop an asymptotic theory of parameter estimation for periodic binary detection processes subject to dead time. Our framework encompasses a wide range of particle and radiation measurement problems in science and engineering (see Section I-A), and we demonstrate its usefulness through an application to lidar (light detection and ranging) [1]–[3], including an example with real (experimental) data. Concretely, the systems we study conduct periodic statistical experiments, each with a binary outcome indicating whether a particle or radiation quantum was detected. From the observed outcomes, one wishes to estimate a physical parameter of interest, such as a pulse time-of-flight in lidar [2] or a lifetime in fluorescence microscopy [4], [5]. A common property of such systems is

that, whenever a detection event occurs, the underlying device enters a “dead-time” period of duration t_d during which no further outcomes can be registered. Such a dead-time interval arises in practice when, for example, particle or radiation detectors are operated in Geiger mode and require a short recovery upon detection before returning to their sensitive state [6]–[10]. To mitigate its effect, experiments are often deliberately activated only during selected time bins, a design choice called *gating*, which trades off conducting the most informative experiments against maximizing the number of experiments [8], [9], [11]–[17]. Together, dead time and gating introduce a systematic discrepancy between the observed and the underlying experimental statistics. In many regimes of practical importance this distortion is statistically significant, and a substantial literature across application domains has proposed empirical correction schemes [6], [8], [9], [18]–[26] (see Section I-B). Previous statistical treatments, however, do not account for the non-i.i.d. stochastic process resulting from dead time and gating (see Section I-C), leaving open both the fundamental lower bounds for this class of problems (which can guide the principled design of estimators and gating schemes) and the efficiency of commonly used estimators. This paper fills that gap.

In Section II, we precisely define periodic “dead-time event detection (DED)” processes to formalize the general class of problems described above, depicted schematically in Figure 1. We identify a sufficient statistic of this process, showing that activation counts can carry information about the physical parameters of interest that hardware-side histogramming typically discards in practice [8], [9], [17], [22]. This observation can inform future hardware histogramming design. In Section III, we develop an asymptotic theory of estimation for DED processes, characterizing the fundamental lower bounds of estimation from dead-time-constrained observations. Using the local asymptotic normality (LAN) framework, we derive the appropriate notion of Fisher information for this non-i.i.d. setting and obtain matching lower bounds through Hájek convolution and local asymptotic minimax theorems. A key consequence of our Fisher-information-rate formula is that the gating rule, even when fully history-dependent, affects asymptotic information only through its limiting phasewise sampling frequencies and, weighted by these frequencies, each sampled phase contributes the usual Bernoulli information. In Section IV, we prove that the maximum likelihood estimator (MLE), of which several implementations are commonly used in practice [9], [18], [21], [25]–[29], is asymptotically efficient.

This work was supported in part by the Singapore-MIT Alliance for Research and Technology (SMART) Wafer-scale Integrated Sensing Devices based on Optoelectronic Metasurfaces (WISDOM) Interdisciplinary Research Group, and by a grant from the Simons Foundation.

F. J. N. Jorgensen and S. G. Johnson are with the Department of Mathematics, Massachusetts Institute of Technology, Cambridge, MA 02139 USA. Corresponding author: F. J. N. Jorgensen; e-mail: fjorgen@mit.edu.

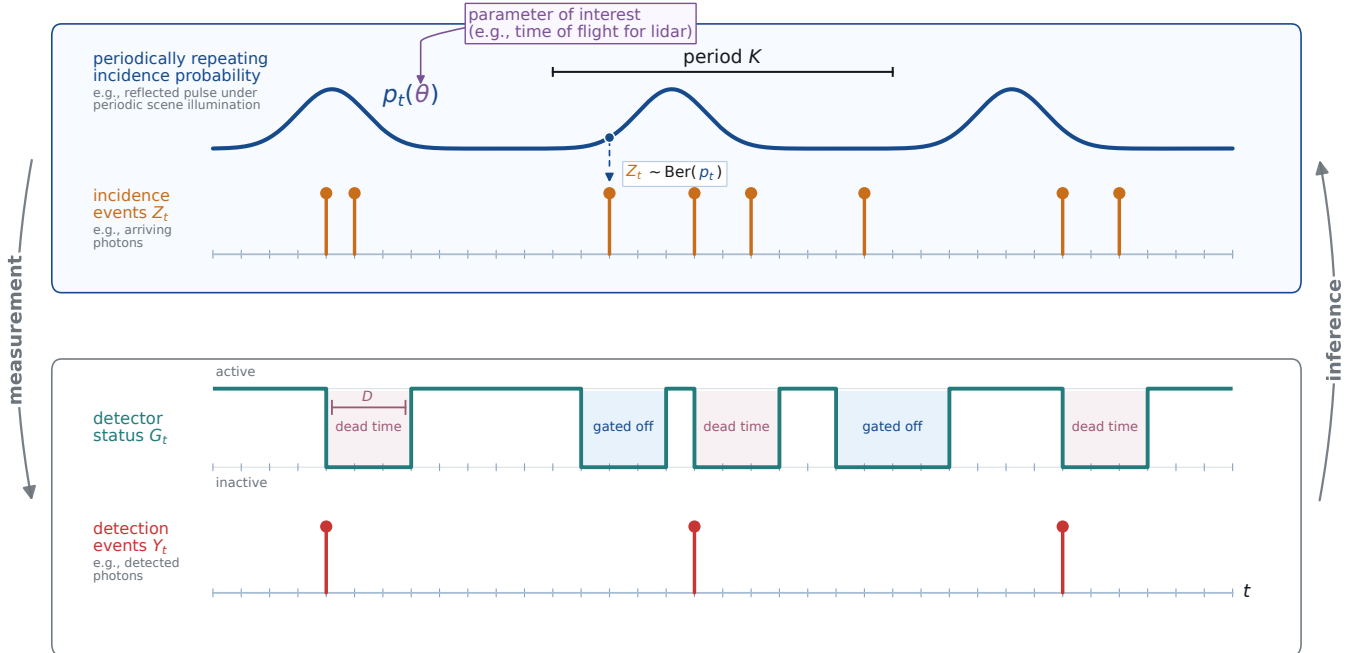


Fig. 1. Schematic of a dead-time event detection (DED) process. The periodic incidence probability $p_t(\theta)$ generates latent Bernoulli incidence events Z_t . The detector status G_t is determined by the gating scheme and dead time. Only incidences occurring while the detector is active are recorded as detections $Y_t = G_t Z_t$, and dead time occurs after every $Y_t = 1$ detection. The goal is to infer θ from the detector data $\{(G_t, Y_t)\}_{t \geq 0}$. In lidar, for example, $p_t(\theta)$ is the photon incidence probability resulting from a repeating return-pulse profile, with θ including the time-of-flight to be estimated from the data.

While prior work has only treated specific gating rules, we further show how to compute the MLE for general gating rules in the dead-time setting. As an alternative to the MLE for estimation from DED processes, we propose a Le Cam one-step update, yielding a class of estimators known as one-step estimators. This class of estimators decouples global parameter localization from locally efficient estimation, where a pilot estimator handles the former and can be designed for stability, robustness, or computational simplicity, while a single update step provides the efficient estimation, which we establish formally. This avoids the pitfalls of nonconvex MLE optimization while retaining its asymptotic efficiency. To illustrate the practical usefulness of these ideas, in Section V we apply the theory to single-photon lidar. We verify that the widely used MLE is asymptotically efficient in this setting, but demonstrate empirically on simulated and real data that one-step estimators (built from a new robust matched-filter pilot we introduce) match the MLE’s efficiency while avoiding both its sensitivity to initialization and its degraded performance under model misspecification. For the specific task of ranging, we apply one-step updates to several estimators from the single-photon lidar literature [22], [25], [30], [31] and show that these corrections substantially improve their performance. We also find that our robust one-step estimator (with only log-linear cost) is competitive with, and arguably outperforms, these corrected literature baselines.

A. Examples of event detection with dead time

DED estimation problems arise in a wide range of physical settings, several of which we briefly describe below. In these applications, the binary event stream records whether at least one particle or radiation quantum was detected in the corresponding time interval.

a) *Single-photon imaging at optical wavelengths:* As single-photon detectors have become more capable and less expensive [7], time-correlated single-photon counting (TC-SPC) has become a widely used technique in a range of imaging applications. In TCSPC, a system is illuminated by a periodic pulse and the statistics of photon arrivals in response to each pulse are used to infer physical parameters of interest [10]. Three representative examples are the following. In lidar [2], [3], each event records the detection of at least one returning photon from an illuminated scene point, and the resulting arrival-time histogram is used to estimate the scene depth and reflectivity at that point. In fluorescence lifetime imaging (FLIM) [4], [5], the recorded events are fluorescence photons whose arrival-rate function decays exponentially after each excitation pulse, and the parameter of interest is an exponential decay constant that corresponds to the fluorescence lifetime of a molecular species. In non-line-of-sight (NLOS) imaging [32]–[34], the detector is scanned over a diffuse relay surface and the photon-arrival rate at each scan position is used to reconstruct a scene hidden around a corner. In all three settings, dead time can systematically distort the observed arrival-time histogram relative to the underlying photon-arrival

distribution [9], [35], [36].

b) Single-photon detection at non-optical wavelengths:

The same model applies to single-photon detectors operating outside the optical spectrum. A prominent example is the estimation of a periodic photon rate using X-ray detectors in astronomy, where the periodicity arises from physical processes such as pulsar rotation [37], [38] or orbiting exoplanets [39].

c) Particle detection: In particle and nuclear physics, and in astroparticle physics, an important application is the estimation of a constant particle or radiation flux from individual detection events [19], [40]–[44].

d) Closely related problems: Several related problems share structural features but violate at least one of the hypotheses of our setting (single detector, event-based, dead-time, periodic). Medical imaging modalities such as positron emission tomography (PET) and computed tomography (CT) employ photon and particle counters described by the same single-detector model [20], [45], but use *arrays* of detectors whose outputs are jointly processed to reconstruct an activity or attenuation distribution inside a body, yielding a multi-dimensional generalization of our problem. A similar multi-detector setup appears in recent work on vibration sensing via frequency-entangled two-photon interference [46], [47], where photon pairs from a Poisson source are routed through an interferometer and their coincidence and anti-coincidence rates at two single-photon detectors encode a time-varying optical delay, which is the parameter to be inferred. Another related problem arises in the neuroscience literature on neural encoding, where a spike-train response (e.g. the action potentials of retinal ganglion cells) is modeled parametrically as a function of a known stimulus, with the goal of estimating the parameters of this model. These models extend our setting in several ways: refractory times, the analogue of dead time in this context, are often nonconstant, and the measured spike-train response may exhibit additional forms of history dependence, referred to in this literature as burstiness and adaptation. Moreover, they frequently, though not always, use aperiodic or stochastic stimuli rather than the periodic setting considered here [48]–[51]. A further related direction concerns refractory periods in models of recurrent event data in medical studies, which are mathematically equivalent to dead time. These typically lack the periodic rate function central to our setting [52]. Refractory-like constraints also arise in queueing applications such as databases and aircraft landings [53], but there the constraint does not restrict what the observer can record and so does not induce the estimation problem studied here. Finally, variability in electromagnetic radiation emitted from accreting galactic black holes and similar astrophysical sources gives rise to a closely related inference problem, but with a stochastic rather than periodic rate function [23].

B. Existing approaches and their limitations

A variety of strategies have been proposed to mitigate dead-time-induced bias in parameter estimation. Although most of these ideas have been developed in the context of lidar and single-photon avalanche diode (SPAD) imaging, the

underlying ideas are general and apply to any dead-time-constrained detection system. Throughout, we use the term *detector* for the device that reads out the binary event of interest, refer to it as *active* when it is able to register an event and *inactive* otherwise.

In low-event-rate regimes, dead-time effects are small and are often simply neglected at the inference stage [3], [10], [54]. Alternatively, computational correction methods can compensate for the dead-time-induced distortion at the inference stage [6], [8], [9], [18]–[25], [36], [55].

A complementary hardware-level approach is *gating*, in which the detector is deliberately activated and deactivated at strategically chosen times to counter pile-up and, potentially, improve temporal resolution and reduce reconstruction error. Representative strategies include activating the detector only over a sub-interval in which signal events are expected [11], [12], and shifting the active window across repeated measurement periods [13]–[16], [56]. *Adaptive* gating uses information from previous measurements to decide when to open the active window [17]. Finally, event-driven or *free-running* acquisition, in which the detector is active whenever it is not in a detection-induced dead-time period, has been studied as an alternative to explicit gating [8], [9].

C. Related work

Despite their empirical success, existing inference methods and gating schemes are motivated by heuristic considerations rather than derived from an explicit statistical framework. Several questions have been left open. To begin with, what notion of Fisher information governs the asymptotic lower bounds for estimation in this setting and do commonly used estimators achieve them? The answers to these questions will also inform how gating schemes should be designed under physical constraints (Section VI). The asymptotic theory of estimation for periodic binary processes *without dead time*, which reduce to product-binomial models, is well-studied [57]–[59]. To the best of our knowledge, however, no analogous theory exists for the dead-time-constrained setting considered here. The dead-time constraint and the gating feedback induce a dependency between successive observations, ruling out a direct application of classical i.i.d. asymptotics. We instead apply local asymptotic normality (LAN) theory [59], [60], which accommodates this dependence structure while still yielding sharp lower bounds and a well-defined notion of asymptotic efficiency.

A related but separate line of work derives lower bounds under the restrictive assumption of *unbiased* estimators, rarely satisfied in practice, either neglecting dead-time effects [16], [21], [61], [62] or restricting to specific forms of gating [63], [64], whereas our LAN-based bounds apply to possibly biased estimators with arbitrary gating.

Notation

We write $\mathbb{N} = \{0, 1, 2, \dots\}$. For $a, b \in \mathbb{R}$, write $a \wedge b := \min\{a, b\}$. For $d \in \mathbb{N}$, \mathbb{R}^d denotes d -dimensional Euclidean space. We write $\|\cdot\|_2$ for the Euclidean norm and $\|\cdot\|_F$ for the Frobenius norm. For a matrix A , $\text{tr}(A)$ denotes its trace

and $\text{diag}(a_1, \dots, a_d)$ the diagonal matrix with diagonal entries a_1, \dots, a_d . For a finite sequence x_0, \dots, x_{T-1} , we use the shorthand $x_{0:T-1} := (x_0, \dots, x_{T-1})$. The law of a random variable X is denoted by $\text{Law}(X)$, and expectation is denoted by \mathbb{E} . For probability measures $P \ll Q$, $D_{\text{KL}}(P||Q) := \mathbb{E}_P[\log(dP/dQ)]$ denotes the Kullback–Leibler divergence. We use \Rightarrow for convergence in distribution and \xrightarrow{P} for convergence in probability under P . $X_T = o_P(1)$ if $X_T \xrightarrow{P} 0$, and $X_T = O_P(1)$ if X_T is bounded in probability.

II. MODEL FORMULATION

We formalize the task of inferring a physical parameter $\theta \in \Theta \subseteq \mathbb{R}^d$ from a periodically repeating sequence of Bernoulli experiments, representing particle or radiation detection events, in which each positive event forces the detector into a *dead-time* period of duration t_d during which no further experiments can be conducted. A second feature we want to capture is *gating*: subject to the dead-time constraint, the experimenter is free to choose *whether* to run an experiment at any given time. The design of gating schemes is important in practical applications because skipping an uninformative experiment preserves the detector’s sensitivity for later, potentially more informative, time intervals [8], [9], [11]–[17], [56].

The remainder of this section is organized as follows. Section II-A defines our observation model and the class of stochastic processes we study, which we call **dead-time event detection (DED)** processes. Section II-B connects this model to concrete applications. Section II-C establishes useful properties of the likelihood, including a sufficient statistic, and connects these results to hardware data compression in bandwidth-limited systems.

A. Observation model

We work in discrete time, $t \in \{0, 1, 2, \dots\} = \mathbb{N}$, with period K a positive integer (see Section II-D for a discussion of this choice). We write $D \in \mathbb{N}$ for the dead-time length in discrete time bins. The underlying physical process has K -periodic event probabilities

$$p_t(\theta) = p_{t+K}(\theta) \in [0, 1] \quad \text{for all } t \in \mathbb{N},$$

depending on the physical parameter $\theta \in \Theta \subseteq \mathbb{R}^d$ that the experimenter wishes to estimate. The corresponding *physical* Bernoulli experiments are sampled independently as

$$Z_t \sim \text{Ber}(p_t(\theta)), \quad t \in \mathbb{N}. \quad (1)$$

In practice, these events correspond to the impingement of at least one particle/radiation quantum. Because of dead time and gating, the experimenter does *not* actually observe the entire sequence $\{Z_t\}_{t \geq 0}$. Instead, the experimental data consist of a stochastic process $\{(G_t, Y_t)\}_{t \geq 0}$ in which $G_t \in \{0, 1\}$ indicates whether an experiment is observed at time t , and the observed outcome is

$$Y_t = G_t Z_t. \quad (2)$$

Thus, Y_t coincides with Z_t whenever the detector is active ($G_t = 1$), while it is identically zero and uninformative about Z_t whenever the detector is inactive ($G_t = 0$).

To fully define the law of $\{(G_t, Y_t)\}_{t \geq 0}$, we must specify how the random variables G_t are chosen. We impose three physical conditions:

a) *Dead-time constraint*: A detected event at time t ($Y_t = 1$) prevents any experimental outcome from being observed over the following D time steps:

$$Y_t = 1 \implies G_s = 0 \text{ for } s \in \{t+1, t+2, \dots, t+D\} \quad (3)$$

almost surely (a.s.). We refer to stochastic processes $\{(G_t, Y_t)\}_{t \geq 0}$ satisfying (3) as *dead-time-constrained*. In Geiger-mode detection experiments, this reflects the recovery time required by the detector after a detection [6].

b) *Gating causality*: Subject to the dead-time constraint, the experimenter is free to choose at any time whether to run an experiment, and a substantial literature has developed proposing schemes for doing so [8], [9], [11]–[17]. To include any such scheme while ruling out an unphysical dependency on future information, we require that for every t there exist $U_t \sim \text{Unif}([0, 1])$, independent of the physical event sequence $\{Z_s\}_{s \geq 0}$ and of the past observations $\{(G_s, Y_s)\}_{s=0}^{t-1}$, and a measurable map $\Phi_t : \{0, 1\}^{2t} \times [0, 1] \rightarrow \{0, 1\}$ such that, a.s.,

$$G_t = \Phi_t(G_0, Y_0, \dots, G_{t-1}, Y_{t-1}, U_t). \quad (4)$$

Equivalently, G_t is drawn from a causal Markov kernel $\pi_t(\cdot \mid G_0, Y_0, \dots, G_{t-1}, Y_{t-1})$ defined as the law of Φ_t . Subject to (3), the choice of the family $\{\Phi_t\}_{t \geq 0}$ constitutes the experimenter’s design freedom. In the following examples, we use the convention that $Y_t = 0$ for $t < 0$. The following two choices are widely used in practice:

- The *free-running* scheme [9], [16], $\Phi_t^{\text{fr}} = 1 - \sum_{s=1}^D Y_{t-s}$, which observes an experiment whenever allowed by the dead-time constraint.
- The *synchronous* scheme [11], [12], in which the detector is activated at the beginning of each period unless still in dead time, and deactivated after the first detection within the period. Writing $m_t := t \bmod K$, this rule is $\Phi_t^{\text{syn}} = \left(1 - \sum_{s=m_t+1}^{m_t+D} Y_{t-s}\right) \left(1 - \sum_{s=1}^{m_t} Y_{t-s}\right)$, with the second sum interpreted as empty when $m_t = 0$.

The trade-off underlying gating design is that not running an experiment reduces the amount of observed data, but can preserve the detector’s sensitivity for subsequent, potentially more informative, time intervals. The statistical framework developed in this paper provides a basis for principled comparison and design of gating schemes $\{\Phi_t\}_{t \geq 0}$ in future work (Section VI).

c) *Gating-frequency convergence*: We require that the empirical frequency of detector activations along each phase stabilizes, meaning that for every $\theta \in \Theta$, there exists a limiting “gating-frequency” vector $\gamma(\theta) \in [0, 1]^K$ such that for each $r = 0, \dots, K-1$,

$$\frac{1}{L} \sum_{\ell=0}^{L-1} G_{r+\ell K} \xrightarrow{P_\theta} \gamma_r(\theta) \quad \text{as } L \rightarrow \infty. \quad (5)$$

When the choice of θ is clear from context, we write γ for $\gamma(\theta)$. Gating-frequency convergence holds for all practical examples we know of and is verified for the free-running and synchronous rules in Appendix A. It could likely be relaxed at the cost of more involved proofs but little additional statistical insight, and schemes that rely on such a relaxation are likely undesirable in practice (see Section III-C).

The following definition collects these requirements and names the class of processes studied in this paper.

Definition 1. A stochastic process $\{(G_t, Y_t)\}_{t \geq 0}$ with $G_t, Y_t \in \{0, 1\}$ is called a **dead-time event detection (DED)** process if it is causal as in (4), gating-frequency convergent as in (5), dead-time-constrained as in (3), and satisfies the observation relations (1)–(2).

The law of a DED process is fully specified by the periodic event probabilities $p_r(\theta)$ and the gating rules $\{\Phi_t\}_{t \geq 0}$ through a simple recursion. The latter determine the conditional law of G_t given the past, and (2) then determines Y_t given G_t .

B. Physical examples

We now connect the abstract model above to concrete physical problems, using single-photon detection as the primary example. Detection of massive particles exhibits the same Poissonian statistics and admits the same argument. In a single-photon counting experiment, $p_t(\theta)$ is the probability that at least one photon arrives in the time bin t . Photon arrival processes are standardly modeled semiclassically as a Poisson point process [65], [66], with a nonnegative photon rate $\lambda_t(\theta) \geq 0$ that is proportional to the classical light intensity. This model is also widely used in the single-photon detection literature [9], [22], [36]. Because a single-photon detector can only register the binary event “at least one photon arrived” (and not the photon number) [7], the detection probability in bin t is

$$p_t(\theta) = 1 - \exp(-\lambda_t(\theta)). \quad (6)$$

The dependence of p_t on θ through the photon rate $\lambda_t(\theta)$ is what makes single-photon detectors useful for parameter θ estimation. We list three important examples.

- **Lidar:** The photon rate $\lambda_t(\theta)$ is a pulse-shaped function of time whose position and amplitude encode, respectively, the round-trip time-of-flight to a scene point and the scene reflectivity, on top of a constant ambient background. The parameter θ collects the time-of-flight, return amplitude, and background level [3], [7]. A detailed treatment is given in Section V.
- **Fluorescence lifetime imaging (FLIM):** Following a short excitation pulse, fluorescent molecules emit photons at an exponentially decaying rate $\lambda_t(\theta)$. The parameter of interest θ in this application is the exponential decay constant called “fluorescence lifetime,” which serves as an important imaging modality in biological experiments [4], [13].
- **X-ray timing in astronomy:** For a periodically varying astrophysical source such as a pulsar or a transiting-exoplanet system, the photon rate $\lambda_t(\theta)$ is a periodic pulse profile whose parameters (e.g. the orbital period, pulse

shape, and pulsed fraction) are the inference targets [37]–[39].

We remark that, in practice, the detection probabilities in (6) also depend on the photon detector efficiency [65], which acts multiplicatively on the photon rate. Without loss of generality, this factor can be absorbed directly into the rate function $\lambda_t(\theta)$, and we omit it from the notation.

C. Likelihood, sufficient statistic, and Rao–Blackwellization

We now derive the likelihood of a DED process up to a finite time horizon $T \in \mathbb{N}$ and identify a sufficient statistic for θ . Writing $X_t := (G_t, Y_t)$, with a feasible realized value $x_t = (g_t, y_t)$, denoting the finite-horizon law by $P_{\theta, T} := \text{Law}(X_{0:T-1})$, writing $\mathbb{E}_{\theta, T}$ for expectation with respect to $P_{\theta, T}$ and suppressing T as in \mathbb{E}_{θ} when the horizon is clear, the chain rule combined with (2), and the definition of π_t yields the factorization

$$P_{\theta, T}(X_{0:T-1} = x_{0:T-1}) = \prod_{t=0}^{T-1} \pi_t(g_t | x_{0:t-1}) \quad (7a)$$

$$\cdot \underbrace{\prod_{t=0}^{T-1} [p_t(\theta)^{y_t} (1 - p_t(\theta))^{1-y_t}]^{g_t}}_{\theta\text{-dependent}}, \quad (7b)$$

where only the second factor depends on θ , and where we use the convention that the bracketed term equals 1 when $g_t = 0$. Define the phasewise aggregate counts

$$N_r(T) := \sum_{\substack{0 \leq t < T \\ t \bmod K = r}} G_t, \quad (8a)$$

$$S_r(T) := \sum_{\substack{0 \leq t < T \\ t \bmod K = r}} Y_t, \quad (8b)$$

for $r = 0, \dots, K-1$, i.e. the number of active bins and the number of detections within phase r up to horizon T . Substituting (8) into (7) gives

$$\log P_{\theta, T}(X_{0:T-1} = x_{0:T-1}) = \sum_{r=0}^{K-1} \left[S_r(T) \log p_r(\theta) \right. \quad (9a)$$

$$\left. + (N_r(T) - S_r(T)) \log(1 - p_r(\theta)) \right] \quad (9b)$$

$$+ C(x_{0:T-1}), \quad (9c)$$

where $C(x_{0:T-1})$ collects θ -independent terms. The following proposition is immediate from the form of (9) and the Neyman–Fisher factorization theorem; see, e.g., Ref. 67.

Proposition 1. For every DED process and every $T \in \mathbb{N}$, the vector of phasewise counts

$$H_T := (N_r(T), S_r(T))_{r=0, \dots, K-1}$$

is sufficient for θ , meaning that the conditional distribution of the full data $X_{0:T-1}$ given H_T does not depend on θ .

Importantly, this implies that any estimator $\hat{\theta}_T$ can be replaced by the conditional expectation $\mathbb{E}[\theta_T | H_T]$, which can be computed without knowing θ by sufficiency, without

increasing the mean squared error at any $\theta \in \Theta$. Therefore, without loss of optimality we may restrict attention to estimators that depend on the data only through H_T . This principle is also known more generally as the Rao–Blackwell theorem [68].

This sufficiency result has direct practical implications for data compression, which is an important problem in modern detection systems such as high-refresh-rate lidar [69]. Proposition 1 tells us that, rather than the full binary stream $\{(G_t, Y_t)\}_{t=0}^{T-1}$, only the $2K$ phasewise counts $(N_r(T), S_r(T))_{r=0}^{K-1}$ need to be stored or transmitted from detector hardware to the inference device. This explicit identification of a sufficient statistic provides a principled basis for ongoing work on hardware data compression in bandwidth-limited systems. Classical histogramming retains only $S_r(T)$ [8], [9], [17], [22], [36]. Depending on the gating scheme used, this *can* be a sufficient statistic. For example, in the free-running case with time horizon $T = LK$, since $G_t = 1 - \sum_{s=1}^D Y_{t-s}$, one has

$$N_r(T) = L - \sum_{s=1}^D S_{(r-s) \bmod K}(T) + O(1) \quad (10)$$

where the $O(1)$ -term is due to boundary effects and negligible as L becomes large. For more general gating schemes where no closed-form expression of the type (10) exists (e.g. adaptive schemes as in Ref. 17), the counts $N_r(T)$ carry additional statistical information that is lost in $S_r(T)$ -histogramming. To our knowledge, this point has not been made explicit in the existing literature. Recent work has empirically proposed retaining $N_r(T)$ alongside $S_r(T)$ for use in a computational correction [70], [71]. Under the free-running scheme used in that work, $N_r(T)$ is determined by $S_r(T)$ up to the boundary correction in (10), so $S_r(T)$ alone would have sufficed asymptotically.

D. Remarks on our modeling assumptions

We make explicit a few of the assumptions underlying the model formulated above and discuss the resulting limitations. First, we assume that the dead time D is known and not part of the parameter θ to be estimated. In practical settings where it is unknown, there is an extensive literature on dead-time estimation developed in nuclear physics, optics, and neuroscience (where the analogous quantity appears as the refractory period in spike trains) [40], [72]–[75].

Second, our exposition adopts the *nonparalyzable* (Type-I) dead-time model, which accurately describes a commonly used class of single-photon detectors, modern single-photon avalanche diodes (SPAD) [76]. A *paralyzable* (Type-II) variant, in which arrivals during an active dead-time interval extend that interval, also appears in the literature and is particularly important for modeling dead time in Geiger–Müller tubes [6], [40]. We leave the analysis of the Type-II model to future work. Our model also accounts only for detector-induced dead time D . In TCSPC systems, an additional timing-electronics dead time can prevent the electronics from registering a new event even after the detector has recovered [77]. This effect is often negligible, for example

when the electronics dead time is shorter than the detector dead time [25], [76], [77].

Finally, we briefly comment on our choice of a discrete-time model. While all digitally acquired data are ultimately discrete, the discretization scale can in principle be made arbitrarily fine. In that regime, the large-sample asymptotics developed in the remainder of this paper may fail to describe the effective statistical behavior, and one could instead consider a joint limit $T, K \rightarrow \infty$ or a continuous-time formulation. We deliberately fix K and let only T grow, which is consistent with the convention in simulations in the existing literature, e.g. for single-photon detection and their associated inference problems [8], [9], [17], [22]. More fundamentally, this has a practical systems-level motivation. In high-flux scenarios with large numbers of events per second such as array-based SPAD architectures [25], [78]–[81], storing and transmitting high-resolution timestamps imposes severe memory and bandwidth constraints. Many modern systems therefore perform relatively *coarse* histogramming (in the sense $K \ll T$) directly at the sensing stage prior to data transmission.

III. ASYMPTOTIC ESTIMATION BOUNDS AND FISHER INFORMATION

We develop a statistical theory of estimation from DED observations $\{(G_t, Y_t)\}_{t=0}^{T-1}$ as defined in Definition 1 in the limit $T \rightarrow \infty$. This asymptotic regime affords tractable analysis and reflects the practical operating conditions in which the available signal is large relative to the number of parameters [3], [5], [38] (see also our previous discussion in Section II-D). In Section III-A we verify that the DED model is locally asymptotically normal (LAN) [59], [60], [82] under mild regularity on the rate function, and identify the corresponding Fisher information rate $\mathcal{I}(\theta; \gamma)$. In Section III-B we use this expansion to derive sharp lower bounds on the asymptotic distribution of estimation errors $\sqrt{T}(\hat{\theta}_T - \theta)$ via the Hájek convolution and local asymptotic minimax theorems.

A. Regularity assumptions and local asymptotic normality of DED processes

Consider a DED process $\{(G_t, Y_t)\}_{t \geq 0}$ with K -periodic event probabilities $p_t(\theta)$ and gating-frequency vector $\gamma(\theta) \in [0, 1]^K$. With X_t and $P_{\theta, T}$ as in Section II-C, we study estimation in the limit $T \rightarrow \infty$. As in (6), we define the rate function $\lambda_t(\theta) \in [0, +\infty]$ by

$$p_t(\theta) = 1 - \exp(-\lambda_t(\theta)),$$

with the convention $\exp(-\infty) = 0$. This reparameterization is fully general and is adopted purely for convenience as in physical applications, $p_t(\theta)$ typically arises from a counting model in which $\lambda_t(\theta)$ is the more natural quantity to work with.

By K -periodicity of $\lambda_t(\theta)$, we write $\lambda_r(\theta)$, $r = 0, \dots, K-1$, for the phasewise rates, so that

$$\lambda_t(\theta) = \lambda_{t \bmod K}(\theta).$$

The phasewise rate vector $(\lambda_r(\theta))_{r=0}^{K-1}$ encodes all of the application-specific physical modeling and will be the central

object on which our regularity assumptions are placed. We make the following assumption on our DED process, which will be used to establish LAN, estimation lower bounds, and the efficiency of several estimators at our true data-generating parameter $\theta_0 \in \Theta$.

Assumption 1. Assume that $\theta_0 \in \text{int}(\Theta)$ and that all of the following hold.

- 1) There exist constants $0 < \lambda_{\min} \leq \lambda_{\max} < \infty$ such that $\lambda_{\min} \leq \lambda_r(\theta) \leq \lambda_{\max}$ for all $r = 0, \dots, K-1$ and all $\theta \in \Theta$.
- 2) For each $r = 0, \dots, K-1$, the map $\lambda_r : \Theta \rightarrow \mathbb{R}$ extends to a C^3 map on an open set containing Θ .
- 3) If $\lambda_r(\theta) = \lambda_r(\theta_0)$ for all r such that $\gamma_r(\theta_0) > 0$, then $\theta = \theta_0$.
- 4) Θ is compact.
- 5) Define the phase-wise Fisher information matrices

$$\mathcal{I}_r(\theta) := \frac{1 - p_r(\theta)}{p_r(\theta)} \nabla \lambda_r(\theta) \nabla \lambda_r(\theta)^\top, \quad (11)$$

For any $\alpha \in [0, 1]^K$, define the information rate

$$\mathcal{I}(\theta; \alpha) := \frac{1}{K} \sum_{r=0}^{K-1} \alpha_r \mathcal{I}_r(\theta). \quad (12)$$

We write the information matrix at the true parameter as

$$\mathcal{I}_0 := \mathcal{I}(\theta_0; \gamma(\theta_0)). \quad (13)$$

Assume that the matrix \mathcal{I}_0 in (13) is positive definite.

Importantly, the form of the Fisher information \mathcal{I}_0 first derived here separates the statistical information in the Bernoulli experiments from the effect of the acquisition rule in (4). The phasewise matrices $\mathcal{I}_r(\theta)$ quantify the information available when phase r is sampled, while the decision rule enters only through the limiting sampling frequencies γ_r . Consequently, for the purpose of asymptotic information calculation, all that matters about the gating rule is how often each phase bin is observed. In many acquisition schemes, these frequencies can be obtained from the stationary law of the induced finite-state process or estimated by Monte-Carlo simulation [9].

Conditions (1), (3), and (5) all serve to ensure that the estimation problem is well-posed. Specifically, Condition (1) rules out non-informative phases in which the detection probability is identically 0 or 1, and gives the global boundedness of the log-likelihood terms used in the MLE consistency proof. Both extremes are physically excluded because an arbitrarily small but nonzero rate is guaranteed by background radiation and intrinsic detector noise (e.g. dark counts in SPADs), and an infinite rate is unphysical [7], [20], [76], [83]. Conditions (3) and (5) are identifiability requirements at two different scales. Condition (3) is a global identifiability statement on the phases that the gating scheme actually visits ($\gamma_r > 0$): if two parameter values produce the same rate on every asymptotically visited phase, the T -scale limiting likelihood cannot distinguish them. Condition (5) ensures that the visited phases carry information along every parameter direction near θ_0 .

Conditions (2) and (4) are technical. The C^3 smoothness in (2) is used to control the remainder in the LAN expansion and could be replaced by weaker differentiability notions (e.g. differentiability in quadratic mean [59]) at the cost of more involved proofs, but we have not pursued this because every rate model we are aware of in the applications of interest is smooth. Compactness of Θ in (4) is invoked in the consistency arguments of Section IV and is similarly stronger than strictly necessary. In practice, however, parameters of interest such as depths, lifetimes, periods, and amplitudes are always known to lie in bounded physical ranges, and we are not aware of a DED application in which estimation over an unbounded parameter space would be meaningful.

Relying on Assumption 1, our strategy is to establish local asymptotic normality (LAN) of DED processes. LAN refers to statistical models whose log-likelihood, rescaled around the true parameter θ_0 at scale $T^{-1/2}$, converges to a quadratic form so that it locally behaves like a Gaussian shift experiment. The curvature of this quadratic form is the Fisher information \mathcal{I}_0 and approximate Gaussianity yields sharp asymptotic lower bounds on estimation error [59], [60].

Proposition 2 (LAN). Suppose Assumption 1 holds at parameter $\theta_0 \in \Theta$. Define the normalized score

$$\Delta_t(\theta_0) := \frac{1}{\sqrt{t}} \sum_{r=0}^{t-1} G_r \frac{Y_r - p_r(\theta_0)}{p_r(\theta_0)} \nabla \lambda_r(\theta_0). \quad (14)$$

Then:

- 1) For every bounded sequence h_t , the local alternatives $P_{\theta_0 + h_t/\sqrt{t}, t}$ and $P_{\theta_0, t}$ are contiguous with respect to each other.
- 2) The following local asymptotic normality (LAN) holds:

$$\begin{aligned} \Lambda_t(\theta_0 + h_t/\sqrt{t}, \theta_0) &:= \log \frac{dP_{\theta_0 + h_t/\sqrt{t}, t}}{dP_{\theta_0, t}} \\ &= h_t^\top \Delta_t(\theta_0) - \frac{1}{2} h_t^\top \mathcal{I}(\theta_0; \gamma) h_t + o_{P_{\theta_0, t}}(1). \end{aligned} \quad (15b)$$

- 3) Under $P_{\theta_0, t}$, $\Delta_t(\theta_0) \Rightarrow \mathcal{N}(0, \mathcal{I}_0)$.

Note that for bounded sequences h_t , we have $\theta_0 + h_t/\sqrt{t} \in \Theta$ for all sufficiently large t , such that the statements above are well-defined. See, e.g., Sec. 3 of Ref. 60 for a formal definition of contiguity and the likelihood ratio employed above. The proof of Proposition 2 is conceptually similar to the i.i.d. case without dead time [59, Theorem 7.2] where $\gamma_r \equiv 1$ and is presented in Appendix C.

B. Lower bounds on estimation

Using standard LAN theory and the expansion in Proposition 2, we can translate the Fisher information rate $\mathcal{I}(\theta; \gamma)$ into sharp lower bounds for estimation in dead-time-constrained experiments. These lower bounds are stated through the Hájek convolution theorem for regular estimators in Theorem 1 and the local asymptotic minimax bound for arbitrary estimators in Theorem 2.

a) *Hájek convolution theorem*: We first state a Hájek convolution theorem for DED processes. This theorem applies to *regular* estimators, meaning estimators whose local asymptotic distribution is stable under perturbations of the true parameter at the $T^{-1/2}$ scale. As a reminder, we give the formal definition following Ref. 60, Section 6, Theorem 3.

Definition 2. A sequence of estimators $(\hat{\theta}_T)_{T \geq 0}$ is called *regular* at θ_0 with limit law \mathcal{L}_{θ_0} on \mathbb{R}^d if, for every fixed sufficiently small $h \in \mathbb{R}^d$,

$$\sqrt{T}(\hat{\theta}_T - \theta_0 - \frac{h}{\sqrt{T}}) \Rightarrow \mathcal{L}_{\theta_0}$$

under $\theta_0 + h/\sqrt{T}$ as $T \rightarrow \infty$.

The regularity condition excludes pathological superefficient behavior at a Lebesgue-null set of parameters $\theta \in \Theta$. For example, a classical theorem of Le Cam implies that for any fixed sequence of estimators $\hat{\theta}_T$ such that $\sqrt{T}(\hat{\theta}_T - \theta)$ has a limit law for each $\theta \in \Theta$, the set of parameter values at which regularity fails is a Lebesgue-null set [60, Chapter 6, Proposition 7]. Thus lower bounds proved for regular estimators apply to arbitrary convergent estimators at Lebesgue-almost every parameter value.

Theorem 1 (Hájek convolution theorem). *Assume the hypotheses of Proposition 2 hold, and let $(\hat{\theta}_T)_{T \geq 0}$ be a regular estimator at θ_0 with limit law \mathcal{L}_{θ_0} as in Definition 2. Then there exists a probability measure ν_{θ_0} on \mathbb{R}^d such that*

$$\mathcal{L}_{\theta_0} = \mathcal{N}(0, \mathcal{I}_0^{-1}) * \nu_{\theta_0}.$$

A short proof by applying LAN and the result of Ref. 60, Section 6, Theorem 3, is given in Appendix C. The theorem says that no regular estimator can have smaller asymptotic spread than $\mathcal{N}(0, \mathcal{I}_0^{-1})$. The following risk bound is an immediate consequence that follows from weak convergence, Portmanteau's Theorem, and the monotone convergence theorem.

Corollary 1. *Assume the hypotheses of Proposition 2 hold. Let $(\hat{\theta}_T)$ be a regular estimator at θ_0 . Then,*

$$\lim_{b \rightarrow \infty} \liminf_{T \rightarrow \infty} \mathbb{E}_{\theta_0} \left[b \wedge T \|\hat{\theta}_T - \theta_0\|_2^2 \right] \geq \text{tr}(\mathcal{I}_0^{-1}) \quad (16)$$

where $x \wedge y := \min\{x, y\}$. This lower bound is achieved if the limit law in Definition 2 is $\mathcal{N}(0, \mathcal{I}_0^{-1})$.

b) *Local minimax bound*: We next give a complementary characterization of the minimal asymptotic estimation error through a local asymptotic minimax result. Unlike the Hájek convolution theorem above, which is stated for regular estimators, the local asymptotic minimax theorem applies to *arbitrary* estimator sequences. It shows that no estimator can uniformly improve on the same Gaussian Fisher information lower bound over shrinking neighborhoods of the true parameter at scale $T^{-1/2}$. The theorem is stated for bowl-shaped loss functions [60]:

Definition 3. A function $W : \mathbb{R}^d \rightarrow [0, \infty)$ is called *bowl-shaped* if for every $a \geq 0$, the sublevel set

$$\{u \in \mathbb{R}^d : W(u) \leq a\}$$

is closed, convex, and symmetric about the origin.

Examples include $W(u) = \|u\|_p^q$ for $p \geq 1$ and $q > 0$, in particular the squared Euclidean loss $W(u) = \|u\|_2^2$.

Theorem 2. *Assume the hypotheses of Proposition 2 hold. Let $W : \mathbb{R}^d \rightarrow [0, \infty)$ be bowl-shaped. Then for every sequence of estimators $(\hat{\theta}_T)$, the following local minimax bound holds*

$$\lim_{b \rightarrow \infty} \lim_{c \rightarrow \infty} \liminf_{T \rightarrow \infty} \sup_{\|\theta - \theta_0\|_2 \leq \frac{c}{\sqrt{T}}} \mathbb{E}_{\theta} \left[b \wedge W \left(\sqrt{T}(\hat{\theta}_T - \theta) \right) \right] \quad (17a)$$

$$\geq \mathbb{E}[W(Z)], \quad (17b)$$

where $Z \sim \mathcal{N}(0, \mathcal{I}_0^{-1})$. In particular,

$$\lim_{b \rightarrow \infty} \lim_{c \rightarrow \infty} \liminf_{T \rightarrow \infty} \sup_{\|\theta - \theta_0\|_2 \leq c/\sqrt{T}} \mathbb{E}_{\theta} \left[b \wedge \left\| \sqrt{T}(\hat{\theta}_T - \theta) \right\|_2^2 \right] \geq \text{tr}(\mathcal{I}_0^{-1}).$$

The proof can be found in Appendix C. The truncation parameter b in Corollary 1 and Theorem 2 can be removed if one cares only about the lower bound and not about its attainment. The Portmanteau Theorem implies that, under the hypotheses of Proposition 2, every sequence of estimators $(\hat{\theta}_T)_{T \geq 0}$ satisfies

$$\lim_{c \rightarrow \infty} \liminf_{T \rightarrow \infty} \sup_{\|\theta - \theta_0\|_2 \leq c/\sqrt{T}} \mathbb{E}_{\theta} \left\| \sqrt{T}(\hat{\theta}_T - \theta) \right\|_2^2 \geq \text{tr}(\mathcal{I}_0^{-1}),$$

together with the analogous statement for Corollary 1. As is standard in asymptotic statistics, we retain the truncation in the stated versions because it ensures the bound is *attained* by any estimator with limit law $\sqrt{T}(\hat{\theta}_T - \theta_0) \Rightarrow \mathcal{N}(0, \mathcal{I}_0^{-1})$. Without truncation, attainment would additionally require passing from convergence in distribution to convergence of second moments, for example via the Vitali convergence theorem by showing uniform integrability of $\left(\left\| \sqrt{T}(\hat{\theta}_T - \theta_0) \right\|_2^2 \right)_{T \geq 0}$.

This justifies restricting the error analysis of estimators $(\hat{\theta}_T)_{T \geq 0}$ in the rest of the paper to the limit law of the error $\sqrt{T}(\hat{\theta}_T - \theta_0)$. An estimator whose error distribution converges to the minimum-spread law $\mathcal{N}(0, \mathcal{I}_0^{-1})$ is asymptotically optimal in the sense of Theorem 1 and Theorem 2 and is called *asymptotically efficient*, or simply *efficient*, in statistics [59], [60]. In the next section, we give two practical examples of efficient estimators for DED processes.

C. On the assumption of gating-frequency convergence

We briefly comment on the role of gating-frequency convergence in Definition 1. The assumption ensures that the acquisition rule has a well-defined asymptotic information rate, which is the quantity entering the lower bounds in Theorem 1 and Theorem 2. One *could* prove these results without this assumption by passing to subsequences along which the empirical gating frequencies converge to some limiting vector γ achieving the liminf risk, and apply the same LAN and lower-bound arguments along this subsequence. We nonetheless impose gating-frequency convergence directly, for three reasons. First, there is no additional statistical insight

when not imposing this assumption. Second, it enables simulation of γ and the empirical computation of asymptotic quantities (as for example in Section IV-B), which would otherwise be practically infeasible. Finally, it is the practically relevant case as practically relevant schemes such as the free-running and synchronous schemes satisfy it (Appendix A). This is natural from an engineering standpoint, since a rule that has not settled asymptotically has no stable answer to the question of which bins are most informative to sample. If the empirical gating frequencies oscillate indefinitely between two limits, for instance, one should restrict to the gating-frequency convergent subsequence achieving the lower asymptotic risk.

IV. EFFICIENT ESTIMATORS

The lower bounds in Corollary 1 and Theorem 2 characterize the best asymptotic performance any estimator can hope to achieve by a limiting mean-zero normal law with covariance \mathcal{I}_0^{-1} . In this section, we will present two concrete implementable estimators that attain these bounds and are hence asymptotically efficient.

In Section IV-A we show asymptotic efficiency of the maximum likelihood estimator (MLE), variants of which are widely used in practical DED applications [9], [18], [21], [25]–[29]. In Section IV-B we introduce one-step estimators for DED processes as a more flexible alternative. Originally popularized by Le Cam, a one-step estimator applies a single local Newton correction to a sufficiently good initial pilot estimator, attaining the same asymptotic efficiency as the MLE while avoiding iterative optimization.

A. Maximum likelihood estimation

Given data X_0, X_1, \dots, X_{T-1} , a maximum likelihood estimator (MLE) is defined as a sequence of estimators $\hat{\theta}_T \in \Theta$ satisfying

$$\begin{aligned} \hat{\theta}_T &\in \arg \max_{\theta \in \Theta} \ell_T(\theta), \\ \ell_T(\theta) &:= \log P_{\theta, T}(X_0, X_1, \dots, X_{T-1}) \end{aligned} \quad (18)$$

for each T , where the explicit form of the likelihood is given in Equation (9). We refer to any such sequence as “the” MLE, although it need not be unique. The MLE is a well-known inference procedure that is widely used in practical applications involving DED processes, though prior work has only addressed specific gating rules [9], [18], [25]–[29]. In contrast, the likelihood formula in Equation (9) enables computation of the MLE for any θ -independent gating rule.

One of the reasons for its popularity is that it is often asymptotically efficient in the i.i.d.-case [59]. The following theorem establishes asymptotic efficiency of the MLE in the non-i.i.d. DED-process case under Assumption 1.

Theorem 3. *Consider the hypotheses of Proposition 2. Write $\mathcal{I}_0 := \mathcal{I}(\theta_0; \gamma(\theta_0))$. Then for any MLE $\hat{\theta}_T$ the following are true.*

- 1) $\hat{\theta}_T$ is consistent, meaning that $\hat{\theta}_T \xrightarrow{P_{\theta_0, T}} \theta_0$.
- 2) It is efficient and, in particular, asymptotically normal $\sqrt{T}(\hat{\theta}_T - \theta_0) \Rightarrow \mathcal{N}(0, \mathcal{I}_0^{-1})$.

- 3) $\hat{\theta}_T$ is regular meaning that for every fixed $h \in \mathbb{R}^d$,

$$\sqrt{T} \left(\hat{\theta}_T - \theta_0 - \frac{h}{\sqrt{T}} \right) \Rightarrow \mathcal{N}(0, \mathcal{I}_0^{-1})$$

under $P_{\theta_0 + h/\sqrt{T}, T}$.

In particular, the MLE achieves the lower bound (16) in the Hájek convolution theorem among regular estimators, and the lower minimax bound (17) among all estimators.

A proof of Theorem 3 can be found in Appendix C. It is worth understanding the intuition behind this result, as it will inform the following discussion. The key is the typical local quadratic structure of the log-likelihood due to LAN (Proposition 2), meaning that in a $T^{-1/2}$ -neighborhood of θ_0 we have informally that

$$\ell_T(\theta) \approx \ell_T(\theta_0) + (\theta - \theta_0)^\top \nabla \ell_T(\theta_0) - \frac{T}{2} (\theta - \theta_0)^\top \mathcal{I}_0 (\theta - \theta_0), \quad (19)$$

so that maximizing the log-likelihood is asymptotically equivalent to maximizing this quadratic. Its maximizer is therefore, approximately,

$$\theta_0 + \mathcal{I}_0^{-1} \nabla \ell_T(\theta_0) / T, \quad (20)$$

which, after rescaling, has the efficient limit law $\mathcal{N}(0, \mathcal{I}_0^{-1})$.

B. One-step estimators

The argument above shows that the MLE achieves efficiency by exploiting the local quadratic LAN-structure of the log-likelihood around θ_0 . Once this structure is recognized, however, the full and typically nonconvex optimization required to compute the MLE is no longer needed.

Replacing θ_0 in (19) by any sufficiently accurate Θ -valued pilot estimator $\tilde{\theta}_T$ such that the quadratic approximation remains valid, the unique maximizer of the resulting quadratic in θ is the explicit Newton update

$$\hat{\theta}_T^{\text{os}} = \tilde{\theta}_T + [\mathcal{I}(\tilde{\theta}_T; \hat{\gamma}_T)]^{-1} \frac{U_T(\tilde{\theta}_T)}{T} \quad (21)$$

if this lies in Θ^1 where $\hat{\gamma}_T$ is an estimator of the limiting gating frequencies γ and $U_T(\tilde{\theta}_T) := \nabla \ell_T(\tilde{\theta}_T)$ is called the *score* in statistics. Intuitively, this estimator should inherit the same efficiency as the MLE since it solves the same local quadratic problem. This general observation in the i.i.d.-setting is due to Le Cam, who introduced the *one-step estimator* as a tool for converting any \sqrt{T} -consistent pilot into an asymptotically efficient procedure [59], [60], [84], [85]. We apply this construction to the DED setting. In particular, we describe how to estimate γ from the gating sequence, how to use this to compute the one-step update, and prove that the resulting estimator inherits the efficient $\mathcal{N}(0, \mathcal{I}_0^{-1})$ limit.

¹Under the assumptions of Theorem 4, this constraint is satisfied with probability tending to one since $\theta_0 \in \text{int}(\Theta)$ and $\tilde{\theta}_T \xrightarrow{P} \theta_0$ in the setting of Theorem 4.

a) *Computing the one-step update (OSE)*: In order to compute the one-step update in (21), we need an estimate of the limiting gating frequencies $\gamma(\theta_0)$ of our DED process. These frequencies can be empirically estimated directly from the observed open-gate indicators. For each phase $r = 0, \dots, K-1$, define

$$\hat{\gamma}_{r,T} = \frac{1}{L} \sum_{\ell=0}^{L-1} G_{r+\ell K}, \quad (22)$$

where $L = \lfloor T/K \rfloor$, and write $\hat{\gamma}_T = (\hat{\gamma}_{0,T}, \dots, \hat{\gamma}_{K-1,T})$. By gating-frequency convergence, $\hat{\gamma}_{r,T} \xrightarrow{P_{\theta_0,T}} \gamma_r(\theta_0)$. Thus the limiting information-rate matrix $\mathcal{I}(\theta_0; \gamma(\theta_0))$ is naturally estimated by $\mathcal{I}(\hat{\theta}_T; \hat{\gamma}_T)$, as we show more formally in the proof later. The one-step estimator can then be computed through the single Newton step in (21). Evaluating $\mathcal{I}(\hat{\theta}_T; \hat{\gamma}_T)$ uses the phasewise sums in (11)–(12) and costs $O(Kd^2)$, while evaluating the score $U_T(\hat{\theta}_T) = \nabla \ell_T(\hat{\theta}_T)$ by differentiating the phasewise likelihood (9) costs $O(Kd)$. The final d -dimensional linear solve in (21) costs $O(d^3)$, so the one-step correction has total cost $O(Kd^2 + d^3)$, or simply $O(K)$ for fixed parameter dimension ($d = 3$ for our lidar example, below).

b) *Asymptotic efficiency*: The following theorem, proved in Appendix C, establishes efficiency of the estimator in (21).

Theorem 4. *Assume the hypotheses of Proposition 2 hold at θ_0 . Let $\hat{\theta}_T$ be any Θ -valued preliminary estimator such that $\sqrt{T}(\hat{\theta}_T - \theta_0) = O_{P_{\theta_0,T}}(1)$ and define $\hat{\theta}_T^{\text{os}}$ as in (21) on the event that $\mathcal{I}(\hat{\theta}_T; \hat{\gamma}_T)$ is invertible, and as $\hat{\theta}_T$ otherwise. Then we have asymptotic efficiency*

$$\sqrt{T}(\hat{\theta}_T^{\text{os}} - \theta_0) \Rightarrow \mathcal{N}(0, \mathcal{I}_0^{-1}).$$

Moreover, for every fixed $h \in \mathbb{R}^d$,

$$\sqrt{T} \left(\hat{\theta}_T^{\text{os}} - \theta_0 - \frac{h}{\sqrt{T}} \right) \Rightarrow \mathcal{N}(0, \mathcal{I}_0^{-1})$$

under $P_{\theta_0+h/\sqrt{T}, T}$. Therefore $(\hat{\theta}_T^{\text{os}})$ is regular at θ_0 with efficient limit law.

This efficiency result shows that the one-step construction has the same asymptotically efficient estimation rate as the MLE. However, there are two other important reasons that make the one-step estimator attractive compared to the MLE. First, computing a one-step update from a closed-form pilot can be cheaper than running a full nonconvex MLE optimization (which in practice often has to be done approximately for speedup [25]). Second, it gives us the freedom to choose the pilot for stability rather than for accuracy, and have the one-step update recover efficiency. This decoupling is particularly valuable because the MLE itself is known to be sensitive to model misspecification [60], [84]–[86]. We will illustrate these advantages empirically in the next section for a DED process arising from lidar, comparing the one-step estimator and MLE more closely.

V. APPLICATION TO LIDAR

We illustrate the theory developed in the previous sections on the important application of single-photon lidar and demonstrate its validity empirically. In lidar, a scene is illuminated

by a periodic train of short laser pulses, and the returning photons are detected by a single-photon detector subject to dead time. The arrival-time statistics of these photons encode the round-trip time-of-flight to the illuminated scene point and the local reflectivity. Importantly, the time-of-flight can be converted to a range if the speed of light c is known in the optical medium. Inferring the time-of-flight, local reflectivity, and sometimes background radiation from photon detection times is the central task in single-photon lidar imaging [3], [7], [9], [25], and the resulting estimates form the basis of three-dimensional reconstruction as used in downstream sensing applications.

A. Statistical model

Lidar is modeled by a DED process with the rate function $\lambda_r(\theta)$ typically taking the form

$$\lambda_r(\theta) = a f_\tau(r) + b, \quad r = 0, \dots, K-1. \quad (23)$$

The parameter to be inferred is $\theta = (a, \tau, b) \in [0, \infty) \times [0, K) \times [0, \infty)$ and the pulse shape is modeled as

$$f_\tau(r) := \int_{\tau-r}^{\tau-r+1} f(x) dx, \quad (24)$$

where $f : \mathbb{R} \rightarrow [0, \infty)$ is a K -periodic time-continuous pulse shape with normalization $\int_0^K f(x) dx = 1$. Here $K \in \mathbb{N}$ is the number of discrete phase bins per laser period, whose physical duration is denoted by t_r . The delay $\tau \in [0, K)$ is the round-trip time-of-flight in phase-bin units, corresponding to physical time $\tau t_r / K$. $a \geq 0$ is the reflectivity, and $b \geq 0$ is a constant background rate due to ambient light and detector dark counts. In practice, the pulse template f can either be determined by measuring the pulse shape of the laser empirically in a calibration step or through approximation with a parametric model [16], [17], [22], [25], [26], [31], [61], [87], [88].

Importantly, although the underlying physical process is continuous in time, the discrete index r in (23) reflects the histogramming that is typically performed in practice with single-photon detectors for bandwidth reasons [25], [26], [78]–[81], see also Section II-D. The statistical problem of estimating θ from DED process data $\{(G_t, Y_t)\}_{t=0}^{T-1}$, therefore, naturally fits into our theory established in Section III and Section IV.

B. Dead-Time-Free and Unbiased Bounds for the Lidar Estimation Problem

We briefly summarize how existing classical theory that neglects dead-time effects [57]–[59] has been applied to lower bounds for estimation in the lidar literature. Most of these results make the approximation that dead-time effects are negligible. Concretely, such bounds have been derived for unbiased estimators of range in a continuous-time model [61] and for unbiased estimators of a constant photon rate in discrete-time models [16], [21], [62]. Besides not accounting for dead time, these results do not characterize fundamental lower bounds for possibly biased estimators as would be typical in practice.

To our knowledge, only two prior works address estimation error under dead time: Daniel and Fessler [89], who derive the

asymptotic mean and variance of the detected photon count under a constant photon rate and free-running acquisition, and Wu et al. [64], who derive the same Fisher information as ours in the lidar-setting but only for the free-running gating scheme and only as a lower bound for unbiased estimators.

C. Theory for asymptotic estimation in lidar

We establish a fundamental estimation lower bound for the lidar problem (23) that accounts for dead time and handles non-constant photon rates. We then verify the conditions of Assumption 1, allowing us to apply the theory from Sections III and IV. We make the following assumptions in addition to the model definition in (24) on the true underlying data-generating parameter θ_0 in our experiment.

- Assumption 2.** 1) The pulse $f : \mathbb{R} \rightarrow [0, \infty)$ is C^3 .
2) Our parameter candidate set $\Theta \subset \mathbb{R}^3$ satisfies $\theta_0 \in \text{int}(\Theta)$ and takes the form

$$\Theta = [a_-, a_+] \times [\tau_-, \tau_+] \times [b_-, b_+],$$

for $0 < a_- < a_+ < \infty$, $0 \leq \tau_- < \tau_+ < K$, and $0 < b_- < b_+ < \infty$.

- 3) The single-photon gating rule Φ_t of the DED process as in (4) is causal, dead-time-constrained, and gating-frequency convergent with limiting gating frequencies $\gamma(\theta_0) \in [0, 1]^K$.
4) For every $\theta \in \Theta$, the active phases identify the true lidar parameter as stated in Assumption 1 (3).
5) Writing $\theta_0 = (a_0, \tau_0, b_0)$ and defining the gradient of

$$\lambda_r(\theta) \text{ as } v_r(\theta_0) := \begin{pmatrix} f_{\tau_0}(r) \\ a_0(f(\tau_0 - r + 1) - f(\tau_0 - r)) \\ 1 \end{pmatrix},$$

the set of vectors $\{v_r(\theta_0) : \gamma_r(\theta_0) > 0\}$ spans \mathbb{R}^3 .

We briefly discuss this assumption. As pointed out in Section III, the C^3 assumption is not strictly necessary, but is easily satisfied by practically used Gaussian pulse models. The upper bounds on a and b reflect finite signal and background levels, and the lower bounds $a_- > 0$ and $b_- > 0$ exclude degenerate regimes where τ is not identifiable and where there is no background radiation. The compactness assumption on τ is purely technical. Since τ is periodic, the natural parameter space is the torus $\mathbb{R}/K\mathbb{Z}$, but we use a compact Euclidean interval to avoid formulating the LAN theory of Section III on manifolds. The proofs use compactness only for uniform bounds on continuous functions, which hold equally on the torus, so all results apply with the torus $\mathbb{R}/K\mathbb{Z}$ in place of $[\tau_-, \tau_+]$. For the free-running and synchronous acquisition rules considered in Section II-A, condition (3) follows from Appendix A. Identifiability in (4) and (5) is necessary for the statistical problem to be well-posed and must be checked for the pulse model used. One can easily verify the following proposition:

Proposition 3. A lidar model satisfying Assumption 2 is a DED process satisfying Assumption 1.

In particular, the correct notion of Fisher information is given by

$$\mathcal{I}(\theta_0; \gamma) = \frac{1}{K} \sum_{r=0}^{K-1} \gamma_r \frac{\exp(-\lambda_r(\theta_0))}{1 - \exp(-\lambda_r(\theta_0))} v_r(\theta_0) v_r(\theta_0)^\top$$

evaluated at the correct gating frequencies, i.e. $\mathcal{I}_0 = \mathcal{I}(\theta_0; \gamma(\theta_0))$. We can directly apply Theorem 1, Theorem 2, Theorem 3, and Theorem 4 in order to conclude the following result.

Corollary 2. Suppose Assumption 2 holds. Then the statements Theorem 1, Theorem 2, Theorem 3, and Theorem 4 hold for the lidar estimation problem, giving the efficient limiting distribution $\mathcal{N}(0, \mathcal{I}_0^{-1})$ and the corresponding Fisher-information lower bounds for regular and local-minimax estimation.

Having proved asymptotic lower bounds and the efficiency of the MLE and one-step estimators, we now discuss practical estimators for lidar in greater detail, both to show how they fit into this picture and to empirically validate the asymptotics at practically meaningful sample sizes.

D. Maximum likelihood and one-step estimators for lidar

In practice, most of the lidar estimation literature is based, either explicitly or implicitly, on maximum likelihood estimation [16], [18], [25], [26], [61], [77], [87], [90], [91]. In our notation, the likelihood is the phasewise likelihood in Equation (18), with

$$p_r(\theta) = 1 - \exp(-\lambda_r(\theta)), \quad \lambda_r(\theta) = a f_{\tau}(r) + b.$$

The corresponding maximum likelihood estimator is

$$\hat{\theta}_T^{\text{MLE}} \in \arg \max_{\theta \in \Theta} \ell_T(\theta). \quad (25)$$

Computing this estimator exactly can be expensive, since the likelihood is generally nonconvex. While some practical methods propose direct computation [26], [92], many practical methods in the literature replace the full joint optimization by faster approximations. One common strategy is to decouple the optimization over τ and (a, b) , for example by using a bilevel optimization procedure [25], [61], [87]. Another strategy is to first estimate the underlying rate profile g by applying the closed-form maximum-likelihood estimator for the underlying intensity, commonly called the Coates-type correction, and then estimate the physical parameters θ from this corrected profile rather than by directly maximizing the likelihood over θ itself [16], [18], [26], [91].

In the experiments below, ‘‘MLE initialized from a pilot’’ refers to the output of a local numerical likelihood optimizer initialized at that pilot, not necessarily to the exact global maximizer in (18). Strictly speaking, the theoretical efficiency result only applies to the latter.

Apart from likelihood-based and likelihood-approximation methods, the only alternative we are aware of that is effective in settings where dead time plays a significant role is based on the method of generalized estimating equations [9]. As this approach has been reported to be more computationally

demanding than maximum-likelihood-based methods without yielding a clear performance advantage [25], we focus here only on maximum likelihood and on new estimators motivated by the one-step construction.

A key observation in Section IV was that the asymptotic efficiency of the MLE comes from the local quadratic structure of the log-likelihood, not from global likelihood maximization itself. The one-step estimator exploits this structure directly by starting from a pilot estimator that is close enough to the true parameter such that a single Newton correction step produces an estimator with the same asymptotic efficiency as the MLE.

Based on this, our theory suggests a different estimator-design principle for the lidar example. Rather than constructing increasingly accurate approximations to the global MLE through iterative optimization, one can construct simple pilot estimators whose only task is to reach the correct local region of the parameter space, and then convert them into efficient estimators by a one-step update. This separates the global localization problem from the local efficiency problem and allows the pilot estimator to be designed for speed, numerical stability, or robustness, rather than as a direct approximation of the MLE. We illustrate this principle by introducing two new pilot estimators.

Both pilot estimators first convert the observed phase counts $(N_r(T), S_r(T))$ as defined in Section II into estimated photon rates through

$$\hat{p}_r = \left(\frac{S_r(T) + 1/2}{N_r(T) + 1} \right), \quad \hat{\lambda}_r = -\log(1 - \hat{p}_r). \quad (26)$$

The 1/2- and 1-offsets regularize the empirical detection frequency and avoid the boundary cases $S_r(T) = 0$ and $S_r(T) = N_r(T)$.²

a) *Fourier inversion estimator*: As a first example, we use a closed-form method-of-moments pilot based on the zeroth and first Fourier modes of the log-transformed rate profile. Let

$$\hat{M}_k = \frac{1}{K} \sum_{r=0}^{K-1} \hat{\lambda}_r \exp(2\pi i k r / K), \quad k = 0, 1.$$

With d_1 denoting the first binned Fourier coefficient of the pulse template, as derived in Appendix B, the Fourier inversion (FI) estimator is $\hat{\theta}_T^{\text{FI}} := (\hat{a}_T^{\text{FI}}, \hat{\tau}_T^{\text{FI}}, \hat{b}_T^{\text{FI}})$, where

$$\hat{a}_T^{\text{FI}} = \frac{|\hat{M}_1|}{|d_1|}, \quad \hat{\tau}_T^{\text{FI}} = \frac{K}{2\pi} \arg \left(\frac{\hat{M}_1}{d_1} \right),$$

$$\hat{b}_T^{\text{FI}} = \hat{M}_0 - \frac{\hat{a}_T^{\text{FI}}}{K}.$$

Here \arg denotes the argument with values in $[0, 2\pi)$, so that $\hat{\tau}_T^{\text{FI}} \in [0, K)$. This estimator is fully explicit and requires no optimization, but it relies on a single harmonic and is therefore sensitive to localized fluctuations or model deviations.

²Equivalently, this is the posterior mean under the Jeffreys prior $p_r \sim \text{Beta}(1/2, 1/2)$ for the binomial detection probability.

b) *Robust matched estimator*: The robust matched estimator uses the same rate estimates but replaces single-harmonic inversion by median-centered template matching. First estimate the background by the phasewise median

$$\hat{b}_T^{(0)} = \text{median}_r \hat{\lambda}_r, \quad J_r = \hat{\lambda}_r - \hat{b}_T^{(0)}.$$

Then estimate the delay by maximizing the circular matched-filter score

$$\hat{\tau}_T^{\text{rob}} \in \arg \max_{j=0, \dots, K-1} C_j, \quad \text{where } C_j = \sum_{r=0}^{K-1} J_r f_j(r). \quad (28)$$

Given this delay estimate, project the centered profile onto the shifted template and re-estimate the background from the median residual:

$$\hat{a}_T^{\text{rob}} = \left(\frac{\sum_{r=0}^{K-1} J_r f_{\hat{\tau}_T^{\text{rob}}}(r)}{\sum_{r=0}^{K-1} f_{\hat{\tau}_T^{\text{rob}}}(r)^2} \right)_+,$$

$$\hat{b}_T^{\text{rob}} = \text{median}_r \left(\hat{\lambda}_r - \hat{a}_T^{\text{rob}} f_{\hat{\tau}_T^{\text{rob}}}(r) \right),$$

where $(x)_+ := \max(x, 0)$. The full estimator is

$$\hat{\theta}_T^{\text{rob}} = \left(\hat{a}_T^{\text{rob}}, \hat{\tau}_T^{\text{rob}}, \hat{b}_T^{\text{rob}} \right).$$

Its main feature is that it uses the full pulse shape rather than only the first Fourier mode, while the two median steps make it less sensitive to localized finite-sample fluctuations and mild background mismatch. A short derivation from robust least squares and matched filtering is given in Appendix B. Similar estimators based on photon arrival quantiles, designed to perform reliably in small-sample regimes and suppress noise-induced detections, have also been proposed in Ref. 90. The correlation-based estimation of τ used here is likewise used often in lidar and frequently incorporated into iterative (approximate) ML algorithms [25], [61], [87]. Moreover, the estimator described here can be computed in $O(K \log K)$ time. The estimates \hat{p} , $\hat{\lambda}$, \hat{a}_T^{rob} , and \hat{b}_T^{rob} require only phasewise operations or sums, and hence are $O(K)$, the median steps are also $O(K)$ [93], and the correlation C_j can be computed with an FFT-based algorithm in $O(K \log K)$ time [93]. As explained in Section IV-B, the subsequent one-step estimate is also $O(K)$.

E. Simulation study

We show how our asymptotic theory manifests in finite samples. In particular, we verify that the MLE and the one-step estimators approach the Fisher-information lower bound at practical horizon sizes, compare their numerical behavior at practically relevant finite horizons, and test their performance against model misspecification.

The pulse shape we will use is a wrapped Gaussian, letting $\phi_\sigma(z) = \frac{1}{\sqrt{2\pi\sigma}} \exp\left(-\frac{z^2}{2\sigma^2}\right)$, and defining

$$f(x) = \sum_{\ell \in \mathbb{Z}} \phi_\sigma(x + \ell K). \quad (29)$$

This wrapped-Gaussian pulse model is standard in single-photon lidar simulations [25], [61], [90]. The binned template $f_\tau(r)$ is then defined as in (24).

We use a physical laser period of $t_r = 100\text{ns}$, divided into $K = 1000$ bins, giving bin width $\Delta = t_r/K = 0.1\text{ns}$. The pulse width is $\sigma = 10$ bins, i.e. $\sigma\Delta = 1\text{ns}$. The true parameter to recover is $\theta_0 = (a_0, \tau_0, b_0) = (1, 370.4, 0.003)$, so the expected signal return is $a_0 = 1$ photon per period and the expected background is $Kb_0 = 3$ photons per period. The dead time is $D = 500$ bins, corresponding to a physical dead time of $t_d = D\Delta = 50\text{ns}$. Under the free-running acquisition scheme, the detector advances by one bin after a miss and by $D + 1$ bins after a detection. These parameter values were chosen as a representative case of the simulation settings commonly used in the single-photon lidar literature [9], [16], [25], [94], [95].

We first validate the asymptotic efficiency of the MLE, in particular subject to different initializations. Since our theory characterizes the efficiency of the MLE, we test it by directly optimizing the joint likelihood (25), as in Ref. 26 and Ref. 92. The optimization is performed in latent variables $\eta = (\eta_a, \eta_\tau, \eta_b)$ using $a = \exp(\eta_a)$, $\tau = \frac{K}{1 + \exp(-\eta_\tau)}$, and $b = \exp(\eta_b)$. This parametrization enforces positivity of a and b , and keeps $\tau \in (0, K)$. Since the true value $\tau_0 = 370.4$ is far from the period boundary, the use of this Euclidean representative of the circular delay does not create a boundary issue in the present experiment. We use the NLOpt implementation of L-BFGS [96], [97], with maximum 1000 objective evaluations, relative parameter tolerance 10^{-8} , and relative objective tolerance 10^{-10} . The optimization is initialized either from the Fourier inversion estimator $\hat{\theta}_T^{\text{FI}}$ or from the robust matched-filter estimator $\hat{\theta}_T^{\text{rob}}$. For an estimator $\hat{\theta}_T = (\hat{a}_T, \hat{\tau}_T, \hat{b}_T)$, we report the relative mean squared error (MSE) through

$$\text{Relative MSE}(a, \tau, b) = \left(\frac{\hat{a}_T - a_0}{a_0} \right)^2 + \left(\frac{d_K(\hat{\tau}_T, \tau_0)}{K} \right)^2 + \left(\frac{\hat{b}_T - b_0}{b_0} \right)^2,$$

where d_K denotes circular distance on the period- K circle. The plotted relative MSE is the Monte-Carlo average of this quantity. In Figure 2, we plot $T\Delta$ times this relative MSE, together with the Fisher-information lower bound

$$\text{tr}(W\mathcal{I}_0^{-1}), \quad W = \Delta \text{diag}(a_0^{-2}, K^{-2}, b_0^{-2}). \quad (30)$$

For comparison, we also plot our Fisher information evaluated at $t_d = 0$ ($\alpha_r \equiv 1$ in (12)) in Figure 2. This recovers the dead-time-free Fisher bound used in prior work [16], [21], [61], [62], where Fisher-information expressions and lower bounds for unbiased estimators were derived only under the assumption of negligible dead time. For the present high-flux parameters, ignoring dead time lowers the bound by about 75.22%, substantially underestimating the minimum attainable error.

This discrepancy becomes small only in a much lower dead time or lower-flux regime. For example, keeping all other parameters fixed, we find numerically that making the dead-time-aware bound exceed the dead-time-free bound by less than 10% requires a dead time of less than approximately 0.46 ns at the nominal flux. Alternatively, if the dead time is

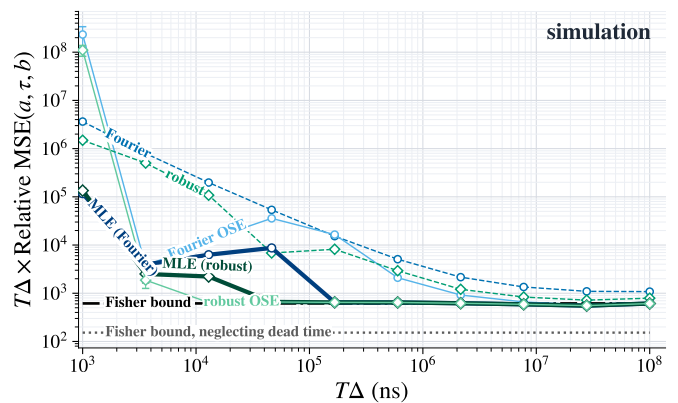


Fig. 2. Mean-square error (MSE) for pulse parameters (a, τ, b) in single-photon lidar simulation scaled by observation time $T\Delta$, comparing various estimators: Fourier and robust pilot estimators (dashed lines), maximum-likelihood estimators (MLE) starting from pilots (thick solid lines), and one-step estimators (OSE) starting from pilots (thin solid lines). Both MLE and OSE approach the Fisher-information lower bound (black line). If dead time is neglected, the Fisher bound is lower (gray line). Error bars (mostly too small to see) are standard error across 10^3 repetitions.

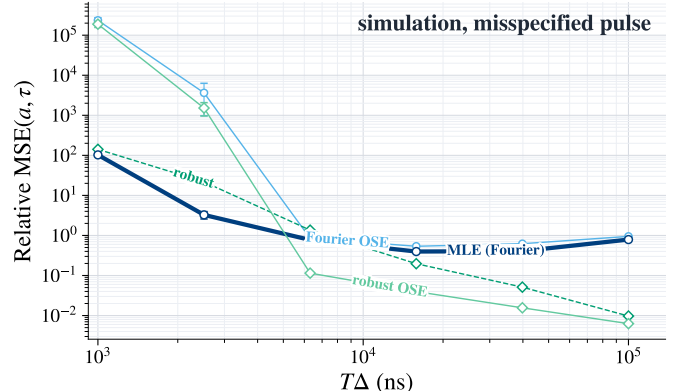


Fig. 3. Relative MSE for pulse parameters (a, τ) in the misspecified single-photon lidar simulation with an added localized background bump in (31), while the fitted estimators still assume the constant-background model from (23). The Fourier-based estimators are strongly affected by the unmodeled bump, and the corresponding MLE/OSE can converge to poor local optima. By contrast, the robust pilot remains stable, and its one-step update gives the lowest error at moderate and large observation times. Error bars are standard error across 10^3 repetitions.

kept at its original value of 50 ns, the entire incident intensity must be scaled by about 0.05, replacing the nominal pulse and background parameters (a_0, b_0) by $(0.05a_0, 0.05b_0)$, to obtain the same 10% gap.

The large-horizon behavior in Figure 2 agrees with the theory at practical time scales: by about $T\Delta = 10^5\text{ns}$, both MLE initializations approach the Fisher-information lower bound. At intermediate horizons, however, the initialization matters substantially. For example, around $T\Delta = 5 \times 10^4\text{ns}$ (which is a very relevant timescale from an applications perspective), the likelihood optimizer initialized from the Fourier-moment pilot is still far from the lower bound while the robust initialization is already very close. This illustrates a practical weakness of the MLE: although it is asymptotically efficient as a statistical procedure, computing it requires a nonconvex

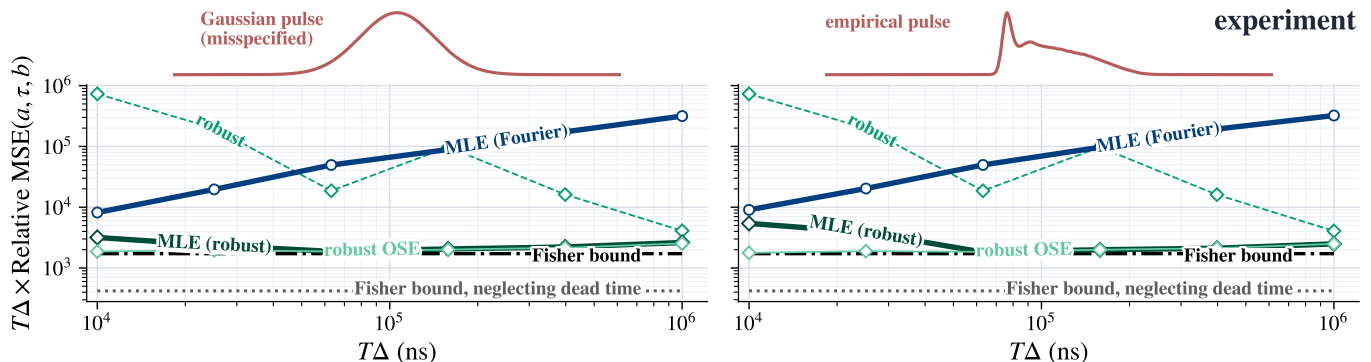


Fig. 4. Real single-photon lidar experiment [77] comparing estimation under a misspecified wrapped-Gaussian pulse model (left) and an experimentally measured pulse model (right). The plotted quantity is $T\Delta$ -scaled relative MSE for (a, τ, b) . The likelihood optimizer initialized from the Fourier estimator fails to reach the efficient regime, whereas the robust-initialized likelihood optimizer and robust one-step estimator yield essentially the same result and remain close to the Fisher-information bound. If dead time is neglected, the Fisher bound is lower. The empirical pulse gives only modest improvement for the robust one-step estimator, indicating limited sensitivity to pulse-shape mismatch. The remaining gap to the bound therefore likely reflects residual experimental nonidealities (e.g., inhomogeneous background, timing jitter, detector effects) not captured by the idealized DED model. The MLE actually performs better under the misspecified wrapped-Gaussian pulse model at short acquisition times, but this difference disappears at longer horizons. Error bars are standard error across 999 blocks.

numerical optimization, and poor initialization can lead to a bad local optimum, in particular at small sample sizes.

As explained in Section IV-B, the one-step estimator avoids a global nonconvex likelihood optimization while retaining asymptotic efficiency. We now test this idea empirically in the same simulation setting as above, using the Fourier-inversion estimator and the robust matched-filter estimator from Section V-D as pilots $\tilde{\theta}_T$, followed by the one-step update

$$\hat{\theta}_T^{\text{os}} = \tilde{\theta}_T + [\mathcal{I}(\tilde{\theta}_T; \hat{\gamma}_T)]^{-1} \frac{U_T(\tilde{\theta}_T)}{T}$$

from (21) with score $U_T(\tilde{\theta}_T) = \nabla \ell_T(\tilde{\theta}_T)$, log-likelihood ℓ_T as defined in (18) and (9), Fisher information $\mathcal{I}(\tilde{\theta}_T; \hat{\gamma}_T)$ as in (12), and empirical gating frequencies $\hat{\gamma}_T$ as in (22).

In Figure 2, the empirical behavior is consistent with the \sqrt{T} -consistent pilot assumption of Theorem 4, which we did not prove mathematically for either pilot. More importantly, the one-step updates recover the Fisher-information bound as predicted by the theory, yielding a substantial improvement over the uncorrected pilot. The Fourier-inversion one-step becomes efficient very late around $T\Delta = 10^7$ ns. The robust matched-filter one-step, on the other hand, reaches the efficient plateau very quickly at about $T\Delta = 10^4$ ns, which is faster than *any* of the MLEs in Figure 2 without requiring the nonconvex optimization. This supports the practical role of the one-step estimators with good pilot estimators as an alternative to the MLE.

We next test robustness of these estimators by introducing a narrow localized background bump to the data-generating photon rate of the previous experiment

$$\lambda_r^{\text{mis}} = a_0 f_{\tau_0}(r) + b_0 + h u_{\tau_b}(r), \quad (31)$$

where $u_{\tau_b}(r)$ is the binned wrapped-Gaussian bump constructed from the Gaussian pulse in (29) analogously to $f_{\tau}(r)$, with parameters $\sigma_b = 1$ and $\tau_b = 70$, normalized to have unit peak, and we use $h = 0.15$. Physically, this could correspond to an unmodeled reflection or inhomogeneous

background counts. The fitted estimators, however, still use the previous model from equation (23). In Figure 3, we report the relative MSE only for the (a, τ) -coordinates, since under this misspecified data-generating model it is ambiguous what the correct constant-background parameter b_0 would be. The MLE initialized from the Fourier-inversion one-step estimate is strongly affected by the unmodeled bump as it converges to bad local minima in the misspecified setting. By contrast, the robust matched-filter pilot remains stable because its median background estimate and template-matching step are less sensitive to localized deviations from the constant-background model. The one-step correction improves the robust pilot. This demonstrates our proposed principle where estimators can be designed with considerations such as robustness in mind, without approximating the MLE, and then refined via a one-step update to convert a good global estimate into one with higher local accuracy and efficiency in the well-specified setting. We provide an additional validation using a real-world dataset to further support these conclusions empirically.

F. Application to real data

We test the discussed estimators on real single-photon lidar data used in Ref. 77 and posted online [83]. We refer the reader to that publication for a complete description of the experimental setup and summarize here the details important for our analysis. The physical laser period is approximately $t_r = 100$ ns, which we aggregate to $K = 625$ phase bins of width $\Delta = 0.16$ ns. The acquisition contains 9,999,925 laser periods. We split it into 999 non-overlapping DED trajectories that are 10,000 periods long. We use their single-pixel ranging measurement 2019_01_28/FGS_td198_2019_01_28_acq14.mat [77, Fig. 5], which contains the detection times from repeated laser returns in a high-flux free-running acquisition with physical dead time $t_d = 198$ ns, corresponding to approximately 1238 aggregated phase bins. For each block and horizon we compute the sufficient statistics

$(N_r(T), S_r(T))_{r=0}^{K-1}$ exactly from the event stream and the known dead time. We estimate the proxy ground-truth parameter $\theta_0 = (a_0, \tau_0, b_0)$ directly from the full acq14 high-flux event stream by maximizing the empirical-pulse likelihood over a , τ , and b , using the experimentally measured laser pulse shape included in the data set. This gives the proxy $\theta_0 = (a_0, \tau_0, b_0) = (0.2620, 17.933, 0.002469)$. As a diagnostic for the profile fit, we also compare the fitted intensity $a_0 f_{\tau_0}(r) + b_0$ with the empirical intensity from (26) weighted by the bin-wise inverse variances, giving an excellent weighted fit with $R^2 = 0.9915$.

We now compare the MLE, the robust estimator, and the robust one-step estimator. To assess robustness, we compute each estimator under two fitted models: the empirically calibrated laser pulse for f in (23), and a misspecified wrapped-Gaussian pulse model as in (29) whose second moment matches that of the calibrated pulse. This is a meaningful experiment because exact calibration data may be inaccessible in applications where environmental changes may affect the pulse shape. Because the delay τ is a continuous parameter, while the calibrated laser pulse is available only as a discrete histogram, we have to interpolate the calibrated pulse before evaluating likelihoods, scores, and Fisher information. After normalizing the pulse samples and forming their empirical CDF, we interpolate with monotone piecewise-cubic Hermite interpolating polynomials (PCHIP), which yield a continuous nonnegative density.³

The results in Figure 4 are consistent with both our theory and the simulation results in Section V-E. We compute the Fisher-information lower bound using (30). For comparison, we also show the bound obtained under the approximation $t_d = 0$, used in previous work [16], [21], [61], [62], which underestimates the minimum attainable error by 75.58%. The robust one-step estimator and the MLE initialized from it closely track the Fisher-information prediction over practically relevant horizons, indicating that our asymptotic theory remains predictive in a realistic acquisition setting, despite unavoidable model mismatch and experimental noise. The MLE initialized from the Fourier-inversion estimator often converges to a poor local optimum and therefore fails to reach the efficient regime.

The data also illustrate the robustness gains of our proposed strategy of pairing the one-step estimator with a good pilot. On the one hand, when the MLE is initialized from the robust estimator, the calibrated-pulse likelihood incurs substantially larger risk at the two smallest horizons, by about 70% and 64%, respectively. This appears to be a finite-sample overfitting effect, against which the misspecified Gaussian pulse acts as a smoother regularizing template. On the other hand, the one-step estimator does not exhibit this pathology. Across all six horizons, its calibrated-pulse risk is 0.6% to 4.8% lower than the Gaussian-pulse version and lower than the MLE, which is notable given how visibly the two pulses differ (Figure 4).

³Since PCHIP interpolation is generally only C^1 , the calibrated-pulse experiment is an empirical diagnostic rather than a literal instance of Assumption 2. Also, we expect the C^3 condition to be stronger than necessary, with differentiability in quadratic mean likely sufficient.

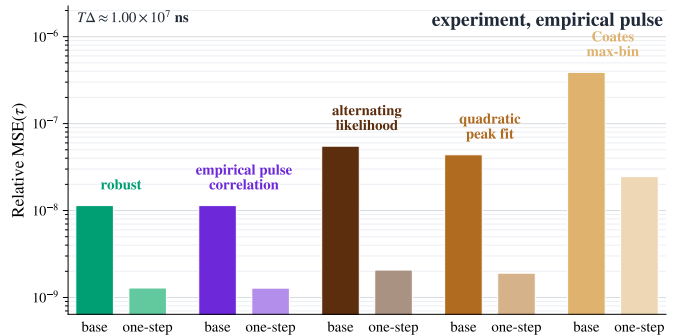


Fig. 5. Relative mean-square error for the delay parameter τ in a real single-photon lidar experiment [77] at the rounded horizon $T\Delta \approx 10^7$ ns using the calibrated empirical pulse. Bars compare each range estimator before correction (“base”) and after one Fisher-scoring one-step update (“one-step”) for our robust pilot, empirical pulse correlation [31], alternating likelihood [25], quadratic peak fitting [30], and Coates max-bin [22]. The one-step update substantially reduces the residual bias of the range-only estimators.

Finally, we apply the one-step estimation idea to several estimators from the single-photon lidar imaging literature and compare them with the robust OSE proposed here. We use our implementations of the alternating-likelihood estimator of Ref. 25, empirical pulse correlation of Ref. 31, quadratic peak fitting of Ref. 30, and Coates max-bin of Ref. 22. Since the latter three methods are range-only estimators and do not estimate (a, b) as required for one-step estimation (21), we fill in these entries by fixing τ at the reported range estimate and maximizing the likelihood in (9) over (a, b) using L-BFGS before applying the one-step update. In contrast, our robust matched estimator provides a direct, optimization-free pilot for all three parameters. Although Ref. 25 use a “censoring-based” estimator to initialize the optimization over (a, τ, b) , our experiments show that the robust pilot is consistently one or more orders of magnitude more accurate than this initializer. We test the one-step updates for these estimators from the literature in the representative calibrated-pulse setting (right side of Figure 4), noting that we observed the same qualitative behavior described in this paragraph in the other scenarios (Figure 2, Figure 3) as well. In Figure 5, we evaluate the relative MSE of the prediction at $T\Delta = 10^7$ ns for the respective base estimator and our proposed one-step update, averaging over 100 non-overlapping trajectories. We observe a significant improvement in prediction performance in all of these cases. We briefly point out why the estimators considered from the literature exhibit such large errors when uncorrected. The empirical pulse correlation and quadratic peak fitting ignore the dead-time-induced histogram distortion, leading to some bias [30], [31].⁴ All of these estimators incur bias because they estimate the peak on the discrete histogramming grid, meaning that they are resolution-limited by the grid. They typically compensate by retaining a high-resolution histogram (at the memory cost discussed in Section II-C) or by taking a few MLE update steps from this as a starting point [22], [25], [30], [31]. Our one-step update is therefore an alternative to

⁴Strictly speaking, these two effects prevent the pilots presented in the exposition from satisfying exact \sqrt{T} -consistency as stated in the asymptotic theory.

iterating MLE steps and complementary to grid refinement, while the robust matched pilot provides an optimization-free way to initialize this correction for the full parameter vector (a, b, τ) .

VI. CONCLUSION

We introduced dead-time event detection (DED) processes to formalize periodic event detection under nonparalyzable dead time, a setting arising in several scientific domains, and developed the corresponding asymptotic theory. In particular, we established local asymptotic normality (LAN) for these models, from which the relevant Fisher-information lower bound and the asymptotic efficiency of both the MLE and one-step estimators follow. Empirically, our lidar experiments, including the real-data example, indicate that the theory is predictive at realistic sample sizes and remains useful under mild model misspecification. The experiments also show the practical appeal of one-step updates as an alternative to MLE optimization for DED processes. A one-step correction substantially improves a range of preliminary estimators, including both the $O(K \log K)$ robust pilot proposed here and several commonly used estimators from the single-photon lidar literature, while requiring only $O(K)$ additional cost and no iterative nonlinear optimization.

Beyond lidar, it would be interesting to apply our theory and proposed one-step correction to other concrete examples, such as fluorescence lifetime imaging [4], [5] or photon rate reconstruction in non-line-of-sight imaging [32]–[34] and quantum vibration sensing [46], [47].

The theory developed here is also useful beyond estimation. The derivation of a sufficient statistic in Proposition 1 and the Fisher information \mathcal{I}_0 in (13) may inform the design and evaluation of lossy data-compression schemes. Moreover, criteria such as minimizing $\text{tr}(\mathcal{I}_0^{-1})$, as suggested by Theorems 1 and 2, can guide the design of gating schemes by optimizing the limiting gating frequencies γ subject to dead-time constraints. We are currently preparing a manuscript addressing this topic.

There are several directions for extending our theoretical results. One is to treat paralyzable (Type II) dead time, where arrivals during the inactive period extend the dead time. Another is statistical testing, which should follow naturally from the LAN formulation and is important in applications such as astrophysics and high-energy physics. Extending the model to multiple spatially coupled parameters or detector arrays would also provide theory for global multipixel reconstruction methods that exploit spatial structure [3], [20], [45]–[47], [87], [91]. Other natural extensions would be to allow model memory beyond dead time (as in the modeling of neurons), as well as stochastic rate functions (which arise in both neuroscience and astrophysical applications) [23], [48]–[51]. It would also be useful to quantify the effect of model misspecification by deriving the limiting error rates of the MLE and one-step estimators under misspecified DED models, extending existing statistical theory for the misspecified setting [98]. In particular, this would provide a theoretical understanding of how sources of error not explicitly accounted for in our model such as

timing jitter and pulse shape misspecification [7], [95] affect estimation performance. Finally, a continuous-time version of our DED framework could connect the present theory to the statistical literature on Poisson processes [99], while extending it to the dead-time-censored single-photon setting considered here.

ACKNOWLEDGMENTS

The authors thank J. Rapp, R. Kitichotkul, and V. K. Goyal for helpful discussions and various pointers into the single-photon detection literature, and B. Horwitz for discussion of neural analogues. ChatGPT was used for proofreading and minor language editing. OpenAI Codex was used to assist software development and figure generation. The authors reviewed all AI-assisted text and code and take full responsibility for the manuscript, computations, and figures. This work was supported in part by the Singapore–MIT Alliance for Research and Technology (SMART) Wafer-scale Integrated Sensing Devices based on Optoelectronic Metasurfaces (WISDOM) interdisciplinary research group, and by a grant from the Simons Foundation.

CODE AVAILABILITY

The analysis and figure-generation code used to produce the plots in this paper is available at <https://github.com/FredericJorgensen/dead-time-event-estimation>.

APPENDIX A

GATING-FREQUENCY CONVERGENCE OF ACQUISITION SCHEMES

We verify gating-frequency convergence for the free-running and synchronous acquisition schemes discussed in Section II-A. For a direct empirical comparison of these schemes we refer the reader to the single-photon detection literature [16], [22], [25], [100]. The argument is pointwise in θ , so throughout this appendix we suppress θ and write $p_r := p_r(\theta)$. We assume $0 < p_r < 1$ for every phase r , as in Assumption 1.

Proposition 4. *The free-running and synchronous acquisition schemes in Section II-A are gating-frequency convergent.*

Proof. Define the dead-time timer $D_t \in \{0, \dots, D\}$ recursively by $D_0 = 0$ and

$$D_{t+1} := \begin{cases} D, & Y_t = 1 \\ (D_t - 1)_+, & Y_t = 0 \end{cases},$$

where $D_t = 0$ means that the detector is available. For free-running acquisition, $G_t = \mathbf{1}_{\{D_t=0\}}$. For synchronous acquisition, define the within-period detection indicator variable W_t , initialized by $W_0 = 0$ and updated by

$$W_{t+1} := \begin{cases} 0, & (t+1) \bmod K = 0 \\ W_t \vee Y_t & \text{otherwise} \end{cases}.$$

Then, writing $q(t) := t - (t \bmod K)$ for the beginning of the period containing t ,

$$G_t = \mathbf{1}_{\{D_{q(t)}=0\}} \mathbf{1}_{\{W_t=0\}}.$$

We have $Y_t = G_t Z_t$ for $(Z_t)_{t \geq 0}$ independent with $Z_t \sim \text{Ber}(p_t)$ in either acquisition scheme.

It suffices to give one argument covering both cases. For either rule, the sampled process

$$\bar{D}_\ell := D_{\ell K}, \quad \ell = 0, 1, \dots,$$

is a time-homogeneous Markov chain on the finite state space $\{0, \dots, D\}$, because the dynamics within each period are identical and the variables (Z_t) are independent with K -periodic probabilities. Since $p_r < 1$ for every phase r , every state can reach 0 with positive probability by observing no detections for sufficiently many periods. Hence every closed communicating class contains 0. Also, 0 has a positive self-loop, since no detection during one full period returns the chain to 0. Thus the reachable skeleton chain has a unique closed aperiodic recurrent class containing 0, and hence a unique stationary distribution μ on that class. The finite-state Markov-chain ergodic theorem gives, for every bounded function f ,

$$\frac{1}{L} \sum_{\ell=0}^{L-1} f(\bar{D}_\ell) \xrightarrow{\text{a.s.}} \sum_{i=0}^D \mu_i f(i).$$

Fix a phase r . For the acquisition rule under consideration, define

$$f_r(i) := \mathbb{E}[G_r \mid D_0 = i],$$

where in the synchronous case we initialize $W_0 = 0$. Let

$$\mathcal{H}_\ell := \sigma(X_0, \dots, X_{\ell K-1}, D_{\ell K})$$

be the information available at the start of the period beginning at ℓK . By K -periodicity and the Markov property, and since in the synchronous case $W_{\ell K} = 0$ at the beginning of every period,

$$\mathbb{E}[G_{r+\ell K} \mid \mathcal{H}_\ell] = f_r(\bar{D}_\ell).$$

Decompose

$$\frac{1}{L} \sum_{\ell=0}^{L-1} G_{r+\ell K} = \frac{1}{L} \sum_{\ell=0}^{L-1} f_r(\bar{D}_\ell) + \frac{1}{L} \sum_{\ell=0}^{L-1} (G_{r+\ell K} - f_r(\bar{D}_\ell)).$$

The first term converges almost surely to $\sum_i \mu_i f_r(i)$. For the second term, note that

$$\mathbb{E}[G_{r+\ell K} - f_r(\bar{D}_\ell) \mid \mathcal{H}_\ell] = 0.$$

If $\ell < v$, the ℓ -th summand is \mathcal{H}_v -measurable, so the cross terms in the variance computation vanish. The summands are bounded by 1, and hence

$$\text{Var} \left(\frac{1}{L} \sum_{\ell=0}^{L-1} (G_{r+\ell K} - f_r(\bar{D}_\ell)) \right) \leq \frac{1}{L^2} \sum_{\ell=0}^{L-1} 1 = O(1/L).$$

Hence the second term is $o_P(1)$. Thus gating-frequency convergence holds with

$$\gamma_r := \sum_{i=0}^D \mu_i f_r(i).$$

Since r was arbitrary, this proves the claim for both acquisition schemes. \square

APPENDIX B

DERIVATION OF THE LIDAR PILOT ESTIMATORS

We give the heuristic derivations behind the two lidar pilot estimators introduced in Section V-D. Both begin from the rate estimates $(\hat{\lambda}_r)_{r=0}^{K-1}$ in (26), for which the log-transform is chosen so that the lidar model becomes additive on the photon-rate scale:

$$\hat{\lambda}_r \approx \lambda_r(\theta) = a f_r(r) + b.$$

A. Fourier inversion estimator

The Fourier inversion estimator is an approximate method-of-moments estimator based on the lowest Fourier modes of $(\hat{\lambda}_r)_{r=0}^{K-1}$. Define

$$\hat{M}_k = \frac{1}{K} \sum_{r=0}^{K-1} \hat{\lambda}_r \exp(2\pi i k r / K), \quad k = 0, 1.$$

Using the approximation $\mathbb{E}(\hat{\lambda}_r) \approx \lambda_r(\theta)$, the corresponding moment equations are

$$\hat{M}_k = \frac{1}{K} \sum_{r=0}^{K-1} \lambda_r(\theta) \exp(2\pi i k r / K), \quad k = 0, 1.$$

For $k = 0$, the normalization of the pulse gives

$$\frac{1}{K} \sum_{r=0}^{K-1} \lambda_r(\theta) = \frac{1}{K} \sum_{r=0}^{K-1} (a f_r(r) + b) = \frac{a}{K} + b.$$

To evaluate the first nonzero Fourier mode, write the Fourier series of the periodic pulse as

$$f(x) = \sum_{m \in \mathbb{Z}} c_m \exp(2\pi i m x / K),$$

$$c_m = \frac{1}{K} \int_0^K f(x) \exp(-2\pi i m x / K) dx.$$

A direct integration over one bin gives

$$f_r(r) = \sum_{m \in \mathbb{Z}} d_m \exp(2\pi i m (\tau - r) / K),$$

$$d_m = c_m \exp(\pi i m / K) \text{sinc} \left(\frac{m}{K} \right). \quad (32)$$

Therefore

$$\frac{1}{K} \sum_{r=0}^{K-1} \lambda_r(\theta) \exp(2\pi i r / K) = a \exp(2\pi i \tau / K) \times \sum_{\ell \in \mathbb{Z}} d_{1+\ell K} \exp(2\pi i \ell \tau),$$

since all Fourier modes except those congruent to 1 modulo K cancel in the discrete sum. We then use the approximation

$$\sum_{\ell \in \mathbb{Z}} d_{1+\ell K} \exp(2\pi i \ell \tau) \approx d_1,$$

which is accurate when the higher Fourier coefficients $d_{1+\ell K}$, $\ell \neq 0$, decay rapidly, for example when f is smooth relative to the binning resolution. This gives the estimator-defining approximate moment equations

$$\hat{M}_0 = \frac{a}{K} + b, \quad \hat{M}_1 = a d_1 \exp(2\pi i \tau / K).$$

Solving these equations yields the Fourier inversion estimator in (27). The coefficient d_1 depends only on the calibrated or modeled pulse template f , and can therefore be precomputed.

B. Robust matched estimator

The robust matched estimator starts from the same approximate additive model

$$\hat{\lambda}_r \approx a f_\tau(r) + b,$$

but avoids reducing the profile to a single Fourier coefficient. Because the pulses used in lidar are narrow, most phases are background-dominated; this motivates the initial robust background estimate

$$\hat{b}_T^{(0)} = \text{median}_r \hat{\lambda}_r, \quad J_r = \hat{\lambda}_r - \hat{b}_T^{(0)}.$$

After centering, the approximate signal model is $J_r \approx a f_\tau(r)$. For a fixed delay τ , the nonnegative least-squares estimate of a is

$$\left(\frac{\sum_{r=0}^{K-1} J_r f_\tau(r)}{\sum_{r=0}^{K-1} f_\tau(r)^2} \right)_+.$$

Thus, when the template norm is fixed or varies slowly with τ , estimating τ reduces to finding the shift with largest matched-filter score as defined in Equation (28) which can be computed efficiently using an FFT. The final formulas in Section V-D then project J onto $f_{\hat{\tau}^{\text{rob}}}$ to estimate a , and re-estimate b as the median residual. The second median step makes the final background estimate robust to localized bins that remain poorly described by the shifted pulse template.

APPENDIX C PROOFS OF MAIN RESULTS

Proof of Proposition 2. All convergences below are under $P_{\theta_0, t}$. The bound on the phasewise rates in Assumption 1 implies that there is $\varepsilon > 0$ such that

$$\varepsilon < p_t(\theta) < 1 - \varepsilon$$

for all $\theta \in \Theta$ and indices t . Therefore, the finite-horizon laws $P_{\theta, t}$, $\theta \in \Theta$, have a common support consisting of the feasible paths compatible with the gating rule and the constraint $G_s = 0 \Rightarrow Y_s = 0$ and the likelihood ratio is well-defined. Define for $r \in \mathbb{N}$, $y \in \{0, 1\}$, and $\theta \in \Theta$

$$\begin{aligned} \varphi_r(y; \theta) &:= p_r(\theta)^y (1 - p_r(\theta))^{1-y}, \\ m_r(y; \theta) &:= \log \varphi_r(y; \theta), \\ s_r(y; \theta) &:= \nabla_\theta m_r(y; \theta), \\ J_r(y; \theta) &:= \nabla_\theta^2 m_r(y; \theta). \end{aligned} \quad (33)$$

Then, the θ -independent gating term cancels out in (7) and we obtain,

$$\log \frac{dP_{\theta, t}}{dP_{\theta_0, t}} = \sum_{r=0}^{t-1} G_r \left(m_r(Y_r; \theta) - m_r(Y_r; \theta_0) \right).$$

Since each λ_r extends to a C^3 map on an open set containing Θ and $p_r(\theta) \in [\varepsilon, 1 - \varepsilon]$, all first, second, and third derivatives of $m_r(y; \theta)$ are uniformly bounded for $r = 0, \dots, K - 1$, $y \in \{0, 1\}$, and $\theta \in \Theta$. Hence, for bounded h_t and with

$\theta_t := \theta_0 + h_t/\sqrt{t}$, Taylor's theorem with uniform remainder gives

$$\begin{aligned} m_r(Y_r; \theta_t) - m_r(Y_r; \theta_0) &= \\ &= \frac{1}{\sqrt{t}} h_t^\top s_r(Y_r; \theta_0) + \frac{1}{2t} h_t^\top J_r(Y_r; \theta_0) h_t + R_{r, t}, \end{aligned}$$

where differential operators refer to the parameter argument and

$$|R_{r, t}| \leq C \frac{\|h_t\|^3}{t^{3/2}}$$

for some constant $C < \infty$ independent of r, t . Summing over $r = 0, \dots, t - 1$ yields

$$\Lambda_t(\theta_0 + h_t/\sqrt{t}, \theta_0) = h_t^\top \Delta_t(\theta_0) + \frac{1}{2} h_t^\top A_t h_t + o(1), \quad (34)$$

where

$$\begin{aligned} \Delta_t(\theta_0) &= \frac{1}{\sqrt{t}} \sum_{r=0}^{t-1} G_r s_r(Y_r; \theta_0), \\ A_t &= \frac{1}{t} \sum_{r=0}^{t-1} G_r J_r(Y_r; \theta_0), \end{aligned}$$

and the $o(1)$ is deterministic, hence also $o_{P_{\theta_0, t}}(1)$. We now identify this with the expression of the score in the statement. Since

$$\nabla p_r(\theta_0) = (1 - p_r(\theta_0)) \nabla \lambda_r(\theta_0),$$

we have

$$\begin{aligned} s_r(y; \theta_0) &= \left(\frac{y}{p_r(\theta_0)} - \frac{1 - y}{1 - p_r(\theta_0)} \right) \nabla p_r(\theta_0) \\ &= \frac{y - p_r(\theta_0)}{p_r(\theta_0)} \nabla \lambda_r(\theta_0). \end{aligned}$$

Thus, $\Delta_t(\theta_0)$ is exactly (14). We bound the quadratic term in order to conclude the asymptotic formula for the likelihoods. Define the filtration

$$\mathcal{F}_r := \sigma(X_0, \dots, X_r, G_{r+1}), \quad r \geq 0,$$

with $\mathcal{F}_{-1} := \sigma(G_0)$. Set

$$\begin{aligned} B_t &:= A_t + \frac{1}{t} \sum_{r=0}^{t-1} G_r \mathcal{I}_r(\theta_0) \\ &= \frac{1}{t} \sum_{r=0}^{t-1} (G_r J_r(Y_r; \theta_0) + G_r \mathcal{I}_r(\theta_0)). \end{aligned}$$

We claim that $B_t \rightarrow 0$ in L^2 , hence $B_t \xrightarrow{P_{\theta_0, t}} 0$. Note first that for $Y \sim \text{Ber}(p_r(\theta_0))$,

$$\begin{aligned} -\mathbb{E}_{\theta_0} [J_r(Y; \theta_0)] &= \mathbb{E}_{\theta_0} [s_r(Y; \theta_0) s_r(Y; \theta_0)^\top] \\ &= \mathcal{I}_r(\theta_0), \end{aligned}$$

by Lemma 1. Consequently,

$$\mathbb{E}_{\theta_0} [G_r J_r(Y_r; \theta_0) + G_r \mathcal{I}_r(\theta_0) \mid \mathcal{F}_{r-1}] = 0.$$

So the summands $Z_r := G_r J_r(Y_r; \theta_0) + G_r \mathcal{I}_r(\theta_0)$ in B_t are martingale differences. $\|Z_r\|_{\mathbb{F}}^2 \leq C'$ is also a.s. bounded by a constant C' (C^3 assumption). Now

$$\begin{aligned} \mathbb{E}_{\theta_0} \|B_t\|_{\mathbb{F}}^2 &= \frac{1}{t^2} \mathbb{E}_{\theta_0} \left\| \sum_{r=0}^{t-1} Z_r \right\|_{\mathbb{F}}^2 \\ &= \frac{1}{t^2} \sum_{r,v=0}^{t-1} \mathbb{E}_{\theta_0} \langle Z_r, Z_v \rangle_{\mathbb{F}}. \end{aligned}$$

If $r < v$, then Z_r is \mathcal{F}_{v-1} -measurable, and therefore by the tower-property of conditional expectation $\mathbb{E}_{\theta_0} \langle Z_r, Z_v \rangle_{\mathbb{F}} = 0$. Hence all cross terms vanish, and so

$$\mathbb{E}_{\theta_0} \|B_t\|_{\mathbb{F}}^2 = \frac{1}{t^2} \sum_{r=0}^{t-1} \mathbb{E}_{\theta_0} \|Z_r\|_{\mathbb{F}}^2 \leq C'/t.$$

Thus $B_t \rightarrow 0$ in L^2 , hence $B_t \xrightarrow{P_{\theta_0,t}} 0$. Further, by gating-frequency convergence, with $L = \lfloor t/K \rfloor$,

$$\frac{1}{t} \sum_{r=0}^{t-1} G_r \mathcal{I}_r(\theta_0) = \mathcal{I}(\theta_0; \gamma) + o_{P_{\theta_0,t}}(1).$$

In particular, $A_t = -\mathcal{I}(\theta_0; \gamma) + o_{P_{\theta_0,t}}(1)$. Substituting this into (34) gives

$$\begin{aligned} \Lambda_t(\theta_0 + h_t/\sqrt{t}, \theta_0) &= \\ &h_t^\top \Delta_t(\theta_0) - \frac{1}{2} h_t^\top \mathcal{I}(\theta_0; \gamma) h_t + o_{P_{\theta_0,t}}(1), \end{aligned}$$

which is exactly (15).

We now prove that $\Delta_t(\theta_0) \Rightarrow \mathcal{N}(0, \mathcal{I}(\theta_0; \gamma))$. By the Cramér–Wold theorem it is sufficient (in fact, necessary) to prove $u^\top \Delta_t(\theta_0) \Rightarrow \mathcal{N}(0, u^\top \mathcal{I}(\theta_0; \gamma) u)$ for all nonzero $u \in \mathbb{R}^d$; the case $u = 0$ is trivial. Define

$$D_r(u) := u^\top G_r s_r(Y_r; \theta_0), \quad r = 0, \dots, t-1.$$

Then

$$u^\top \Delta_t(\theta_0) = \frac{1}{\sqrt{t}} \sum_{r=0}^{t-1} D_r(u).$$

Set

$$\sigma_u^2 := u^\top \mathcal{I}(\theta_0; \gamma) u.$$

By positive definiteness of $\mathcal{I}(\theta_0; \gamma)$, $\sigma_u^2 > 0$. For each t , define a scalar martingale-difference array by

$$\xi_{t,r} := \frac{D_r(u)}{\sqrt{t} \sigma_u}, \quad \mathcal{G}_{t,r} := \mathcal{F}_r, \quad r = 0, \dots, t-1.$$

Since G_r is \mathcal{F}_{r-1} -measurable and

$$\mathbb{E}_{\theta_0} [s_r(Y_r; \theta_0) \mid \mathcal{F}_{r-1}] = 0 \quad \text{on } \{G_r = 1\},$$

while $D_r(u) = 0$ on $\{G_r = 0\}$, we have

$$\mathbb{E}_{\theta_0} [\xi_{t,r} \mid \mathcal{G}_{t,r-1}] = 0.$$

Thus $\{\xi_{t,r}, \mathcal{G}_{t,r}\}_{r=0}^{t-1}$ is a martingale-difference array. Next, its conditional variance satisfies

$$\begin{aligned} V_t^2 &:= \sum_{r=0}^{t-1} \mathbb{E}_{\theta_0} [\xi_{t,r}^2 \mid \mathcal{G}_{t,r-1}] \\ &= \frac{1}{t \sigma_u^2} \sum_{r=0}^{t-1} \mathbb{E}_{\theta_0} [D_r(u)^2 \mid \mathcal{F}_{r-1}] \\ &= \frac{1}{t \sigma_u^2} u^\top \left(\sum_{r=0}^{t-1} G_r \mathcal{I}_r(\theta_0) \right) u \xrightarrow{P_{\theta_0,t}} 1, \end{aligned}$$

by our shown convergence of the empirical Fisher information. Finally, since $p_r(\theta_0) \in [\varepsilon, 1 - \varepsilon]$ and the phase set is finite, there exists $C_u < \infty$ such that

$$|D_r(u)| \leq C_u \quad \text{a.s. for all } r.$$

Hence, for every $\delta > 0$,

$$|\xi_{t,r}| \leq \frac{C_u}{\sqrt{t} \sigma_u} < \delta$$

for all sufficiently large t , uniformly in r . Therefore

$$\sum_{r=0}^{t-1} \mathbb{E}_{\theta_0} [\xi_{t,r}^2 \mathbf{1}_{\{|\xi_{t,r}| > \delta\}} \mid \mathcal{G}_{t,r-1}] = 0$$

for all sufficiently large t , so the conditional Lindeberg condition holds. By the scalar martingale central limit theorem [101, Theorem 4]

$$\frac{u^\top \Delta_t(\theta_0)}{\sigma_u} = \sum_{r=0}^{t-1} \xi_{t,r} \Rightarrow \mathcal{N}(0, 1),$$

which shows the claimed normality result.

We conclude the proof by proving contiguity. To prove contiguity, take any subsequence. It has a further subsequence along which $h_t \rightarrow h \in \mathbb{R}^d$ (we avoid relabeling). Along that subsubsequence, by Slutsky's theorem

$$\begin{aligned} \Lambda_t(\theta_0 + h_t/\sqrt{t}, \theta_0) &\Rightarrow h^\top Z - \frac{1}{2} h^\top \mathcal{I}(\theta_0; \gamma) h, \\ Z &\sim \mathcal{N}(0, \mathcal{I}(\theta_0; \gamma)). \end{aligned}$$

By the continuous mapping theorem,

$$\begin{aligned} \exp\left(\Lambda_t(\theta_0 + h_t/\sqrt{t}, \theta_0)\right) &\Rightarrow \exp\left(h^\top Z - \frac{1}{2} h^\top \mathcal{I}(\theta_0; \gamma) h\right). \end{aligned}$$

This limit has expectation 1 and is almost surely strictly positive. Therefore, by Le Cam's first lemma, $P_{\theta_0 + h_t/\sqrt{t}, t}$ and $P_{\theta_0, t}$ are mutually contiguous. \square

Lemma 1. *Let $Y \sim \text{Ber}(p_r(\theta))$ in the setting of Proposition 2. With the notation from (33), we have*

$$-\mathbb{E}_\theta [J_r(Y; \theta)] = \mathbb{E}_\theta [s_r(Y; \theta) s_r(Y; \theta)^\top] = \mathcal{I}_r(\theta).$$

Proof. Since

$$\nabla m_r(y; \theta) = \frac{y - p_r(\theta)}{p_r(\theta)(1 - p_r(\theta))} \nabla p_r(\theta),$$

we obtain

$$\begin{aligned} \mathbb{E}_\theta [\nabla m_r(Y; \theta) \nabla m_r(Y; \theta)^\top] &= \frac{\text{Var}_\theta(Y)}{p_r(\theta)^2 (1 - p_r(\theta))^2} \nabla p_r(\theta) \nabla p_r(\theta)^\top \\ &= \frac{1}{p_r(\theta) (1 - p_r(\theta))} \nabla p_r(\theta) \nabla p_r(\theta)^\top. \end{aligned}$$

On the other hand, a direct differentiation of

$$m_r(y; \theta) = y \log p_r(\theta) + (1 - y) \log(1 - p_r(\theta))$$

and taking expectations using $\mathbb{E}_\theta[Y] = p_r(\theta)$ gives

$$-\mathbb{E}_\theta[\nabla^2 m_r(Y; \theta)] = \frac{1}{p_r(\theta) (1 - p_r(\theta))} \nabla p_r(\theta) \nabla p_r(\theta)^\top.$$

Finally, since

$$\nabla p_r(\theta) = (1 - p_r(\theta)) \nabla \lambda_r(\theta),$$

both expressions equal

$$\frac{1 - p_r(\theta)}{p_r(\theta)} \nabla \lambda_r(\theta) \nabla \lambda_r(\theta)^\top = \mathcal{I}_r(\theta).$$

□

Proof of Theorem 1. Define the estimator of the local parameter $\hat{h}_T := \sqrt{T}(\hat{\theta}_T - \theta_0)$. By regularity, $\hat{h}_T - h \Rightarrow \mathcal{L}_{\theta_0}$ under $P_{\theta_0 + h/\sqrt{T}, T}$, independently of h . By Proposition 2 and the Hájek convolution theorem [60, Theorem 3], we therefore have

$$\mathcal{L}_{\theta_0} = \mathcal{N}(0, \mathcal{I}_0^{-1}) * \nu_{\theta_0}$$

for some probability measure ν_{θ_0} on \mathbb{R}^d . □

Proof of Theorem 2. Given an estimator $\hat{\theta}_T$, pass to the local parametrization

$$h = \sqrt{T}(\theta - \theta_0), \quad \hat{h}_T = \sqrt{T}(\hat{\theta}_T - \theta_0).$$

Then

$$\sqrt{T}(\hat{\theta}_T - \theta) = \hat{h}_T - h.$$

By Proposition 2, the local experiments around θ_0 converge in the LAN sense with information matrix \mathcal{I}_0 . Therefore the hypotheses of the local asymptotic minimax theorem [60, Section 6.6, Theorem 1] are satisfied. Applying that theorem to the local estimator \hat{h}_T and substituting back $h = \sqrt{T}(\theta - \theta_0)$ gives (17). □

Proof of Theorem 3. Using the phase counts $N_r(T), S_r(T)$ from Section II-C and (8), we have

$$\begin{aligned} \ell_T(\theta) &= \sum_{r=0}^{K-1} \left[S_r(T) \log p_r(\theta) \right. \\ &\quad \left. + (N_r(T) - S_r(T)) \log(1 - p_r(\theta)) \right]. \end{aligned}$$

We can ignore the θ -independent part here because it has no impact on the maxima of $\ell_T(\theta)$. Set $p_r^0 := p_r(\theta_0)$ and define

$$M_r(T) := S_r(T) - p_r^0 N_r(T) = \sum_{\substack{0 \leq t < T \\ t \bmod K = r}} G_t(Y_t - p_r^0).$$

Because G_t is predictable and, for $t \bmod K = r$, conditional on $G_t = 1$ we have $Y_t \sim \text{Ber}(p_r^0)$, the increments of

$M_r(T)$ are bounded martingale differences with respect to our filtration \mathcal{F}_t from before. Hence cross-terms vanish and we can expand the diagonal terms as

$$\mathbb{E}_{\theta_0} M_r(T)^2 = \sum_{\substack{0 \leq t < T \\ t \bmod K = r}} \mathbb{E}_{\theta_0} [G_t p_r^0 (1 - p_r^0)] \leq T,$$

so $M_r(T)/T \rightarrow 0$ in L^2 , hence $M_r(T)/T \xrightarrow{P_{\theta_0, T}} 0$. Together with gating-frequency convergence,

$$\begin{aligned} \frac{S_r(T)}{T} &\xrightarrow{P_{\theta_0, T}} \frac{\gamma_r(\theta_0) p_r^0}{K}, \\ \frac{N_r(T) - S_r(T)}{T} &\xrightarrow{P_{\theta_0, T}} \frac{\gamma_r(\theta_0) (1 - p_r^0)}{K}. \end{aligned}$$

Since $\log p_r(\theta)$ and $\log(1 - p_r(\theta))$ are uniformly bounded on Θ by Condition (1) in Assumption 1, we obtain

$$\sup_{\theta \in \Theta} \left| \frac{\ell_T(\theta)}{T} - m(\theta) \right| \xrightarrow{P_{\theta_0, T}} 0,$$

where

$$m(\theta) := \frac{1}{K} \sum_{r=0}^{K-1} \gamma_r(\theta_0) \left[p_r^0 \log p_r(\theta) + (1 - p_r^0) \log(1 - p_r(\theta)) \right].$$

Moreover, defining $R_+ := \{r : \gamma_r(\theta_0) > 0\}$, we have

$$\begin{aligned} m(\theta) - m(\theta_0) &= -\frac{1}{K} \sum_{r \in R_+} \gamma_r(\theta_0) \\ &\quad \cdot D_{\text{KL}}(\text{Ber}(p_r^0) \parallel \text{Ber}(p_r(\theta))) \\ &\leq 0, \end{aligned}$$

with equality if and only if $p_r(\theta) = p_r(\theta_0)$ for all $r \in R_+$ by (3) in Assumption 1 and injectivity of $\lambda \mapsto 1 - \exp(-\lambda)$. In particular, θ_0 is the unique maximizer of m and by continuity of m and compactness of Θ , $\sup_{\theta \in \Theta: \|\theta - \theta_0\|_2 \geq \varepsilon} m(\theta) < m(\theta_0)$

for every $\varepsilon > 0$. Therefore, Theorem 5.7 of Ref. 59 yields

$$\hat{\theta}_T \xrightarrow{P_{\theta_0, T}} \theta_0.$$

This shows consistency.

Next, to show asymptotic normality, use the notation introduced in (33). Then

$$\begin{aligned} \nabla \ell_T(\theta) &= \sum_{t=0}^{T-1} G_t s_t(Y_t; \theta), \\ \nabla^2 \ell_T(\theta) &= \sum_{t=0}^{T-1} G_t J_t(Y_t; \theta). \end{aligned}$$

At θ_0 ,

$$T^{-1/2} \nabla \ell_T(\theta_0) = \Delta_T(\theta_0).$$

By Proposition 2,

$$\Delta_T(\theta_0) \Rightarrow \mathcal{N}(0, \mathcal{I}_0).$$

Work on the event that $\hat{\theta}_T$ and the line segment from $\hat{\theta}_T$ to θ_0 lie in the interior of Θ . Because θ_0 is an interior point and $\hat{\theta}_T$

is consistent, this event has probability tending to one. Next, define

$$\bar{J}_T := -\frac{1}{T} \int_0^1 \nabla^2 \ell_T(\theta_0 + u(\hat{\theta}_T - \theta_0)) du.$$

By the fundamental theorem of calculus,

$$\nabla \ell_T(\hat{\theta}_T) = \nabla \ell_T(\theta_0) - T \bar{J}_T(\hat{\theta}_T - \theta_0). \quad (35)$$

Note that by the phasewise rates extending to C^3 maps on an open set containing Θ , $J_t(y; \cdot)$ is Lipschitz on Θ , uniformly in t and $y \in \{0, 1\}$, with a constant L_Θ . Set $\delta_T := \hat{\theta}_T - \theta_0$. Applying this fact and the triangle inequality gives

$$\begin{aligned} \|\bar{J}_T + T^{-1} \nabla^2 \ell_T(\theta_0)\|_F &\leq T^{-1} \int_0^1 \left\| \nabla^2 \ell_T(\theta_0 + u\delta_T) \right. \\ &\quad \left. - \nabla^2 \ell_T(\theta_0) \right\|_F du \\ &\leq T^{-1} \sum_{t=0}^{T-1} \int_0^1 G_t L_\Theta u \|\delta_T\|_2 du \\ &\leq L_\Theta \int_0^1 u \|\delta_T\|_2 du \\ &\leq L_\Theta \|\delta_T\|_2. \end{aligned}$$

Together with $\delta_T = o_{P_{\theta_0, T}}(1)$, this bound implies

$$\|\bar{J}_T + T^{-1} \nabla^2 \ell_T(\theta_0)\|_F = o_{P_{\theta_0, T}}(1).$$

As shown in the proof of Proposition 2, $-\frac{1}{T} \nabla^2 \ell_T(\theta_0) = \mathcal{I}_0 + o_{P_{\theta_0, T}}(1)$, and therefore we can conclude that

$$\bar{J}_T = \mathcal{I}_0 + o_{P_{\theta_0, T}}(1).$$

The first-order condition for the interior maximizer gives $\nabla \ell_T(\hat{\theta}_T) = 0$. Combining this with (35), we get

$$0 = \nabla \ell_T(\theta_0) - T \bar{J}_T(\hat{\theta}_T - \theta_0).$$

Multiplying by $1/\sqrt{T}$ implies that

$$o_{P_{\theta_0, T}}(1) = \Delta_T(\theta_0) - \bar{J}_T \sqrt{T}(\hat{\theta}_T - \theta_0). \quad (36)$$

By $\bar{J}_T = \mathcal{I}_0 + o_{P_{\theta_0, T}}(1)$, \bar{J}_T is invertible with probability tending to 1, and we can invert (36) to get

$$\sqrt{T}(\hat{\theta}_T - \theta_0) = \bar{J}_T^{-1} \Delta_T(\theta_0) + o_{P_{\theta_0, T}}(1). \quad (37)$$

Now, Slutsky's theorem gives

$$\sqrt{T}(\hat{\theta}_T - \theta_0) \Rightarrow \mathcal{N}(0, \mathcal{I}_0^{-1}).$$

Finally, we show regularity using Le Cam's third lemma and (37). Fix $h \in \mathbb{R}^d$. By Proposition 2 we also have that

$$\log \frac{dP_{\theta_0+h/\sqrt{T}, T}}{dP_{\theta_0, T}} = h^\top \Delta_T(\theta_0) - \frac{1}{2} h^\top \mathcal{I}_0 h + o_{P_{\theta_0, T}}(1).$$

Since $\Delta_T(\theta_0) \Rightarrow \mathcal{N}(0, \mathcal{I}_0)$ under $P_{\theta_0, T}$, by Slutsky we get the joint convergence

$$\begin{aligned} \left(\begin{array}{c} \Delta_T(\theta_0) \\ \log \frac{dP_{\theta_0+h/\sqrt{T}, T}}{dP_{\theta_0, T}} \end{array} \right) &\Rightarrow \mathcal{N}(\mu_h, \Sigma_h), \\ \mu_h &:= \begin{pmatrix} 0 \\ -\frac{1}{2} h^\top \mathcal{I}_0 h \end{pmatrix}, \\ \Sigma_h &:= \begin{pmatrix} \mathcal{I}_0 & \mathcal{I}_0 h \\ h^\top \mathcal{I}_0 & h^\top \mathcal{I}_0 h \end{pmatrix} \end{aligned}$$

under $P_{\theta_0, T}$. Le Cam's third lemma now yields

$$\Delta_T(\theta_0) \Rightarrow \mathcal{N}(\mathcal{I}_0 h, \mathcal{I}_0)$$

under $P_{\theta_0+h/\sqrt{T}, T}$. We want to substitute this into the linearization (37). Note that by contiguity, the $o_{P_{\theta_0, T}}(1)$ becomes $o_{P_{\theta_0+h/\sqrt{T}, T}}(1)$ and therefore \bar{J}_T also has the same limit. In equations, this means that

$$\sqrt{T} \left(\hat{\theta}_T - \theta_0 - \frac{h}{\sqrt{T}} \right) = \mathcal{I}_0^{-1} \Delta_T(\theta_0) - h + o_{P_{\theta_0+h/\sqrt{T}, T}}(1),$$

where we also subtracted h on both sides. Slutsky's theorem concludes the proof

$$\sqrt{T} \left(\hat{\theta}_T - \theta_0 - \frac{h}{\sqrt{T}} \right) \Rightarrow \mathcal{N}(0, \mathcal{I}_0^{-1}).$$

□

Proof of Theorem 4. Since $\sqrt{T}(\tilde{\theta}_T - \theta_0) = O_{P_{\theta_0, T}}(1)$, we have $\tilde{\theta}_T \xrightarrow{P_{\theta_0, T}} \theta_0$. Because each λ_r extends to a C^3 map on an open set containing Θ and is bounded away from 0 and ∞ on Θ , the maps $\theta \mapsto \mathcal{I}_r(\theta)$ are L -Lipschitz on Θ , with constant $L > 0$ uniformly in $r = 0, \dots, K-1$. First we show that the empirical Fisher at the pilot is consistent.

$$\begin{aligned} \|\mathcal{I}(\tilde{\theta}_T; \hat{\gamma}_T) - \mathcal{I}(\theta_0; \hat{\gamma}_T)\| & \\ &\leq \frac{1}{K} \sum_{r=0}^{K-1} \hat{\gamma}_{r, T} L \|\tilde{\theta}_T - \theta_0\| \leq L \|\tilde{\theta}_T - \theta_0\|, \end{aligned}$$

and hence,

$$\mathcal{I}(\tilde{\theta}_T; \hat{\gamma}_T) = \mathcal{I}(\theta_0; \hat{\gamma}_T) + o_{P_{\theta_0, T}}(1).$$

By gating-frequency convergence, $\mathcal{I}(\theta_0; \hat{\gamma}_T) = \mathcal{I}_0 + o_{P_{\theta_0, T}}(1)$ and, therefore,

$$\mathcal{I}(\tilde{\theta}_T; \hat{\gamma}_T) = \mathcal{I}_0 + o_{P_{\theta_0, T}}(1).$$

Since \mathcal{I}_0 is positive definite, $\mathcal{I}(\tilde{\theta}_T; \hat{\gamma}_T)$ is invertible with probability tending to 1. Using the exact same argument as the one following (35) in the proof of Theorem 3 and defining \bar{J}_T with $\tilde{\theta}_T$ instead of $\hat{\theta}_T$, we get the expansion

$$U_T(\tilde{\theta}_T) = U_T(\theta_0) - T \bar{J}_T(\tilde{\theta}_T - \theta_0)$$

with $\bar{J}_T = \mathcal{I}_0 + o_{P_{\theta_0, T}}(1)$. Since $T^{-1/2} U_T(\theta_0) = \Delta_T(\theta_0)$, this becomes

$$\frac{1}{\sqrt{T}} U_T(\tilde{\theta}_T) = \Delta_T(\theta_0) - \bar{J}_T \sqrt{T}(\tilde{\theta}_T - \theta_0).$$

Substituting into the definition of $\hat{\theta}_T^{\text{os}}$,

$$\begin{aligned} \sqrt{T}(\hat{\theta}_T^{\text{os}} - \theta_0) &= \sqrt{T}(\tilde{\theta}_T - \theta_0) \\ &\quad + [\mathcal{I}(\tilde{\theta}_T; \hat{\gamma}_T)]^{-1} \frac{1}{\sqrt{T}} U_T(\tilde{\theta}_T) \\ &= [\mathcal{I}(\tilde{\theta}_T; \hat{\gamma}_T)]^{-1} \Delta_T(\theta_0) \\ &\quad + \left[I_d - [\mathcal{I}(\tilde{\theta}_T; \hat{\gamma}_T)]^{-1} \times \bar{J}_T \right] \\ &\quad \times \sqrt{T}(\tilde{\theta}_T - \theta_0). \end{aligned}$$

Now Proposition 2 gives $\Delta_T(\theta_0) = O_{P_{\theta_0,T}}(1)$, the assumption gives $\sqrt{T}(\hat{\theta}_T - \theta_0) = O_{P_{\theta_0,T}}(1)$, and we already proved

$$\begin{aligned} [\mathcal{I}(\hat{\theta}_T; \hat{\gamma}_T)]^{-1} &= \mathcal{I}_0^{-1} + o_{P_{\theta_0,T}}(1), \\ I_d - [\mathcal{I}(\hat{\theta}_T; \hat{\gamma}_T)]^{-1} \bar{J}_T &= o_{P_{\theta_0,T}}(1). \end{aligned}$$

Hence

$$\sqrt{T}(\hat{\theta}_T^{\text{os}} - \theta_0) = \mathcal{I}_0^{-1} \Delta_T(\theta_0) + o_{P_{\theta_0,T}}(1).$$

Proposition 2 further yields

$$\Delta_T(\theta_0) \Rightarrow \mathcal{N}(0, \mathcal{I}_0),$$

so Slutsky's theorem gives

$$\sqrt{T}(\hat{\theta}_T^{\text{os}} - \theta_0) \Rightarrow \mathcal{N}(0, \mathcal{I}_0^{-1}).$$

Fix now $h \in \mathbb{R}^d$. By Proposition 2, $P_{\theta_0+h/\sqrt{T},T}$ is contiguous with respect to $P_{\theta_0,T}$. Therefore every $o_{P_{\theta_0,T}}(1)$ term above is also $o_{P_{\theta_0+h/\sqrt{T},T}}(1)$, and so

$$\sqrt{T}(\hat{\theta}_T^{\text{os}} - \theta_0) = \mathcal{I}_0^{-1} \Delta_T(\theta_0) + o_{P_{\theta_0+h/\sqrt{T},T}}(1).$$

As in the proof of Theorem 3, by Proposition 2 and Le Cam's third lemma,

$$\Delta_T(\theta_0) \Rightarrow \mathcal{N}(\mathcal{I}_0 h, \mathcal{I}_0) \quad \text{under } P_{\theta_0+h/\sqrt{T},T}.$$

Therefore,

$$\begin{aligned} \sqrt{T} \left(\hat{\theta}_T^{\text{os}} - \theta_0 - \frac{h}{\sqrt{T}} \right) &= \mathcal{I}_0^{-1} \Delta_T(\theta_0) - h + o_{P_{\theta_0+h/\sqrt{T},T}}(1) \\ &\Rightarrow \mathcal{N}(0, \mathcal{I}_0^{-1}). \end{aligned}$$

This is exactly regularity at θ_0 with limit law $\mathcal{N}(0, \mathcal{I}_0^{-1})$. \square

REFERENCES

- [1] G. Fiocco and L. Smullin, "Detection of scattering layers in the upper atmosphere (60–140 km) by optical radar," *Nature*, vol. 199, no. 4900, pp. 1275–1276, 1963.
- [2] P. Dong and Q. Chen, *LiDAR Remote Sensing and Applications*. CRC Press, 2017.
- [3] A. Kirmani, D. Venkatraman, D. Shin, A. Colaço, F. N. Wong, J. H. Shapiro, and V. K. Goyal, "First-photon imaging," *Science*, vol. 343, no. 6166, pp. 58–61, 2014.
- [4] W. Becker, A. Bergmann, M. Hink, K. König, K. Benndorf, and C. Biskup, "Fluorescence lifetime imaging by time-correlated single-photon counting," *Microscopy Research and Technique*, vol. 63, no. 1, pp. 58–66, 2004.
- [5] W. Becker, "Fluorescence lifetime imaging—techniques and applications," *Journal of Microscopy*, vol. 247, no. 2, pp. 119–136, 2012.
- [6] J. W. Müller, "Dead-time problems," *Nuclear Instruments and Methods*, vol. 112, no. 1-2, pp. 47–57, 1973.
- [7] G. S. Buller and R. J. Collins, "Single-photon generation and detection," *Measurement Science and Technology*, vol. 21, no. 1, p. 012002, 2010.
- [8] S. Isbaner, N. Karedla, D. Ruhlandt, S. C. Stein, A. Chizhik, I. Gregor, and J. Enderlein, "Dead-time correction of fluorescence lifetime measurements and fluorescence lifetime imaging," *Optics Express*, vol. 24, no. 9, pp. 9429–9445, 2016.
- [9] J. Rapp, Y. Ma, R. M. Dawson, and V. K. Goyal, "Dead time compensation for high-flux ranging," *IEEE Transactions on Signal Processing*, vol. 67, no. 13, pp. 3471–3486, 2019.
- [10] D. V. O'Connor and D. Phillips, *Time-Correlated Single Photon Counting*. Academic Press, 1984.
- [11] M. Buttafava, G. Bosco, A. Ruggeri, A. Dalla Mora, and A. Tosi, "Time-gated single-photon detection module with 110 ps transition time and up to 80 MHz repetition rate," *Review of Scientific Instruments*, vol. 85, no. 8, p. 083114, 2014.
- [12] M. Buttafava, J. Zeman, A. Tosi, K. Eliceiri, and A. Velten, "Non-line-of-sight imaging using a time-gated single photon avalanche diode," *Optics Express*, vol. 23, no. 16, pp. 20997–21011, 2015.
- [13] X. F. Wang, T. Uchida, D. M. Coleman, and S. Minami, "A two-dimensional fluorescence lifetime imaging system using a gated image intensifier," *Applied Spectroscopy*, vol. 45, no. 3, pp. 360–366, 1991.
- [14] A. Tosi, A. Dalla Mora, F. Zappa, A. Gulinatti, D. Contini, A. Pifferi, L. Spinelli, A. Torricelli, and R. Cubeddu, "Fast-gated single-photon counting technique widens dynamic range and speeds up acquisition time in time-resolved measurements," *Optics Express*, vol. 19, no. 11, pp. 10735–10746, 2011.
- [15] D. Reilly and G. Kanter, "High speed lidar via GHz gated photon detector and locked but unequal optical pulse rates," *Optics Express*, vol. 22, no. 13, pp. 15718–15723, 2014.
- [16] A. Gupta, A. Ingle, and M. Gupta, "Asynchronous single-photon 3D imaging," in *Proceedings of the IEEE/CVF International Conference on Computer Vision*, 2019, pp. 7909–7918.
- [17] R. Po, A. Pediredla, and I. Gkioulekas, "Adaptive gating for single-photon 3D imaging," in *Proceedings of the IEEE/CVF Conference on Computer Vision and Pattern Recognition (CVPR)*, 2022, pp. 16354–16363.
- [18] P. Coates, "The correction for photon 'pile-up' in the measurement of radiative lifetimes," *Journal of Physics E: Scientific Instruments*, vol. 1, no. 8, p. 878, 1968.
- [19] S. H. Lee and R. P. Gardner, "A new G–M counter dead time model," *Applied Radiation and Isotopes*, vol. 53, no. 4-5, pp. 731–737, 2000.
- [20] K. Taguchi, M. Zhang, E. C. Frey, X. Wang, J. S. Iwanczyk, E. Nygard, N. E. Hartsough, B. M. Tsui, and W. C. Barber, "Modeling the performance of a photon counting X-ray detector for CT: energy response and pulse pileup effects," *Medical Physics*, vol. 38, no. 2, pp. 1089–1102, 2011.
- [21] A. K. Pediredla, A. C. Sankaranarayanan, M. Buttafava, A. Tosi, and A. Veeraraghavan, "Signal processing based pile-up compensation for gated single-photon avalanche diodes," 2018. [Online]. Available: <https://arxiv.org/abs/1806.07437>
- [22] A. Gupta, A. Ingle, A. Velten, and M. Gupta, "Photon-flooded single-photon 3D cameras," in *Proceedings of the IEEE/CVF Conference on Computer Vision and Pattern Recognition (CVPR)*, 2019, pp. 6770–6779. [Online]. Available: https://openaccess.thecvf.com/content_CVPR_2019/html/Gupta_Photon-Flooded_Single-Photon_3D_Cameras_CVPR_2019_paper.html
- [23] D. Huppenkothen and M. Bachetti, "Accurate X-ray timing in the presence of systematic biases with simulation-based inference," *Monthly Notices of the Royal Astronomical Society*, vol. 511, no. 4, pp. 5689–5708, 2022.
- [24] M. L. Larsen and A. B. Kostinski, "Simple dead-time corrections for discrete time series of non-Poisson data," *Measurement Science and Technology*, vol. 20, no. 9, p. 095101, 2009.
- [25] R. Kitichotkul, S. Bharadwaj, J. Rapp, Y. Ma, A. Mehta, and V. K. Goyal, "Free-running vs. synchronous: Single-photon lidar for high-flux 3d imaging," in *Proceedings of the IEEE/CVF International Conference on Computer Vision (ICCV)*, 2025, pp. 25972–25982. [Online]. Available: https://openaccess.thecvf.com/content/ICCV2025/html/Kitichotkul_Free-running_vs_Synchronous_Single-Photon_Lidar_for_High-flux_3D_Imaging_ICCV_2025_paper.html
- [26] X. Wang, Y. Kang, T. Zhang, L. Li, W. Kang, and W. Zhao, "Synchronous single-photon lidar ranging with up to two triggers per pulse cycle," *Optics Express*, vol. 34, no. 3, pp. 3816–3827, 2026.
- [27] M. Maus, M. Cotlet, J. Hofkens, T. Gensch, F. C. De Schryver, J. Schaffer, and C. Seidel, "An experimental comparison of the maximum likelihood estimation and nonlinear least-squares fluorescence lifetime analysis of single molecules," *Analytical Chemistry*, vol. 73, no. 9, pp. 2078–2086, 2001.
- [28] A. Chessel, F. Waharte, J. Salamero, and C. Kervrann, "A maximum likelihood method for lifetime estimation in photon counting-based fluorescence lifetime imaging microscopy," in *21st European Signal Processing Conference (EUSIPCO 2013)*. IEEE, 2013, pp. 1–5.
- [29] Ž. Bajzer, T. M. Therneau, J. C. Sharp, and F. G. Prendergast, "Maximum likelihood method for the analysis of time-resolved fluorescence decay curves," *European Biophysics Journal*, vol. 20, no. 5, pp. 247–262, 1991.
- [30] A. M. Pawlikowska, A. Halimi, R. A. Lamb, and G. S. Buller, "Single-photon three-dimensional imaging at up to 10 kilometers range," *Optics Express*, vol. 25, no. 10, pp. 11919–11931, 2017.
- [31] A. McCarthy, X. Ren, A. Della Frera, N. R. Gemmill, N. J. Krichel, C. Scarcella, A. Ruggeri, A. Tosi, and G. S. Buller, "Kilometer-range

- depth imaging at 1550 nm wavelength using an InGaAs/InP single-photon avalanche diode detector,” *Optics Express*, vol. 21, no. 19, pp. 22 098–22 113, 2013.
- [32] R. J. Drost, B. M. Sadler, and G. Chen, “Dead time effects in non-line-of-sight ultraviolet communications,” *Optics Express*, vol. 23, no. 12, pp. 15 748–15 761, 2015.
- [33] J. Rapp, C. Saunders, J. Tachella, J. Murray-Bruce, Y. Altmann, J.-Y. Tourneret, S. McLaughlin, R. M. Dawson, F. N. Wong, and V. K. Goyal, “Seeing around corners with edge-resolved transient imaging,” *Nature Communications*, vol. 11, no. 1, p. 5929, 2020.
- [34] D. Faccio, A. Velten, and G. Wetzstein, “Non-line-of-sight imaging,” *Nature Reviews Physics*, vol. 2, no. 6, pp. 318–327, 2020.
- [35] Z. Li, J. Lai, C. Wang, W. Yan, and Z. Li, “Influence of dead-time on detection efficiency and range performance of photon-counting laser radar that uses a Geiger-mode avalanche photodiode,” *Applied Optics*, vol. 56, no. 23, pp. 6680–6687, 2017.
- [36] L. Xu, Y. Zhang, Y. Zhang, L. Wu, C. Yang, X. Yang, Z. Zhang, and Y. Zhao, “Signal restoration method for restraining the range walk error of Geiger-mode avalanche photodiode lidar in acquiring a merged three-dimensional image,” *Applied Optics*, vol. 56, no. 11, pp. 3059–3063, 2017.
- [37] M. Weisskopf, B. Brinkman, C. Canizares, G. Garmire, S. Murray, and L. Van Speybroeck, “An overview of the performance and scientific results from the Chandra X-ray Observatory,” *Publications of the Astronomical Society of the Pacific*, vol. 114, no. 791, pp. 1–24, 2002.
- [38] Y. Tuo, X. Li, Y. Tan, B. Wu, W. Jiang, L. Song, J. Qu, S. Gogate, S.-N. Zhang, and A. Santangelo, “Revisiting the dead time effects of Insight-HXMT/ME on timing analysis,” *Monthly Notices of the Royal Astronomical Society*, vol. 532, no. 4, pp. 4317–4325, 2024.
- [39] K. Poppenhaeger, J. Schmitt, and S. Wolk, “Transit observations of the hot Jupiter HD 189733b at X-ray wavelengths,” *The Astrophysical Journal*, vol. 773, no. 1, p. 62, 2013.
- [40] G. F. Knoll, *Radiation Detection and Measurement*. John Wiley & Sons, 2010.
- [41] F. Gesualdi and A. D. Supanitsky, “Estimation of the number of counts on a particle counter detector with full time resolution,” *The European Physical Journal C*, vol. 82, no. 10, p. 925, 2022.
- [42] The Pierre Auger Collaboration, “The Pierre Auger Observatory Upgrade—preliminary design report,” Fermi National Accelerator Laboratory, Tech. Rep. FERMILAB-DESIGN-2016-05, 2016. [Online]. Available: <https://arxiv.org/abs/1604.03637>
- [43] F. Reines, C. L. Cowan, Jr., F. B. Harrison, and D. S. Carter, “Detection of neutrons with a large liquid scintillation counter,” *Review of Scientific Instruments*, vol. 25, no. 11, pp. 1061–1070, 1954.
- [44] L. Pál and I. Pázsit, “On some problems in the counting statistics of nuclear particles: Investigation of the dead time problems,” *Nuclear Instruments and Methods in Physics Research Section A: Accelerators, Spectrometers, Detectors and Associated Equipment*, vol. 693, pp. 26–50, 2012.
- [45] E. Vicente, J. L. Herraiz, S. España, E. Herranz, M. Desco, J. J. Vaquero, and J. M. Udías, “Improved dead-time correction for PET scanners: application to small-animal PET,” *Physics in Medicine & Biology*, vol. 58, no. 7, pp. 2059–2072, 2013.
- [46] C. P. Lualdi, J. Rapp, and P. G. Kwiat, “Quantum-enhanced sensing of time-varying signals at the nanometer scale,” in *Quantum Sensing, Imaging, and Precision Metrology IV*, vol. 13920. SPIE, 2026, p. 139200I.
- [47] C. P. Lualdi, S. J. Johnson, M. Vayninger, K. A. Meier, S. Sahoo, S. I. Bogdanov, and P. G. Kwiat, “Fast quantum interferometry at the nanometer and attosecond scales with energy-entangled photons,” *Science Advances*, vol. 11, no. 21, 2025.
- [48] J. W. Pillow, J. Shlens, L. Paninski, A. Sher, A. M. Litke, E. J. Chichilnisky, and E. P. Simoncelli, “Spatio-temporal correlations and visual signalling in a complete neuronal population,” *Nature*, vol. 454, no. 7207, pp. 995–999, 2008.
- [49] J. Keat, P. Reinagel, R. C. Reid, and M. Meister, “Predicting every spike: A model for the responses of visual neurons,” *Neuron*, vol. 30, no. 3, pp. 803–817, 2001.
- [50] L. McIntosh, N. Maheswaranathan, A. Nayebi, S. Ganguli, and S. Baccus, “Deep learning models of the retinal response to natural scenes,” in *Advances in Neural Information Processing Systems*, vol. 29, 2016, pp. 1369–1377. [Online]. Available: <https://proceedings.neurips.cc/paper/2016/hash/a1d33d0dfec820b41b54430b50e96b5c-Abstract.html>
- [51] M. J. Berry and M. Meister, “Refractoriness and neural precision,” in *Advances in Neural Information Processing Systems*, vol. 10, 1997, pp. 110–116. [Online]. Available: <https://proceedings.neurips.cc/paper/1997/hash/95151403b0db4f75bfd8da0b393af853-Abstract.html>
- [52] A. Jahn-Eimermacher, K. Ingel, A.-K. Ozga, S. Preussler, and H. Binder, “Simulating recurrent event data with hazard functions defined on a total time scale,” *BMC Medical Research Methodology*, vol. 15, no. 1, p. 16, 2015.
- [53] H. P. Galliher and R. C. Wheeler, “Nonstationary queuing probabilities for landing congestion of aircraft,” *Operations Research*, vol. 6, no. 2, pp. 264–275, 1958.
- [54] B. Valeur and M. N. Berberan-Santos, *Molecular Fluorescence: Principles and Applications*. Wiley-VCH, 2012.
- [55] A. Hou, Y. Hu, N. Zhao, J. Fang, S. Xu, and Q. Zhou, “Full-waveform fast correction method for photon counting Lidar,” *Chinese Optics Letters*, vol. 19, no. 5, p. 052701, 2021.
- [56] A. Pifferi, A. Torricelli, L. Spinelli, D. Contini, R. Cubeddu, F. Martelli, G. Zaccanti, A. Tosi, A. Dalla Mora, F. Zappa, and S. Cova, “Time-resolved diffuse reflectance using small source-detector separation and fast single-photon gating,” *Physical Review Letters*, vol. 100, no. 13, p. 138101, 2008.
- [57] R. H. Berk, “Consistency and asymptotic normality of MLE’s for exponential models,” *The Annals of Mathematical Statistics*, pp. 193–204, 1972.
- [58] B. Efron, *Exponential Families in Theory and Practice*. Cambridge University Press, 2022, vol. 16.
- [59] A. W. van der Vaart, *Asymptotic Statistics*, ser. Cambridge Series in Statistical and Probabilistic Mathematics. Cambridge University Press, 1998, vol. 3.
- [60] L. Le Cam and G. L. Yang, *Asymptotics in Statistics: Some Basic Concepts*. Springer Science & Business Media, 2000.
- [61] R. Kitichotkul, J. Rapp, and V. K. Goyal, “The role of detection times in reflectivity estimation with single-photon lidar,” *IEEE Journal of Selected Topics in Quantum Electronics*, vol. 30, no. 1, pp. 8 800 114:1–14, 2024.
- [62] Y. M. Lu, “Adaptive sensing and inference for single-photon imaging,” in *2013 47th Annual Conference on Information Sciences and Systems (CISS)*. IEEE, 2013, pp. 1–6.
- [63] T. Rebafka, F. Roueff, and A. Soulloumiac, “Information bounds and MCMC parameter estimation for the pile-up model,” *Journal of Statistical Planning and Inference*, vol. 141, no. 1, pp. 1–16, 2011.
- [64] H. Wu, Y. Wang, S. Sun, L. Zhao, L. Tong, L. Shen, and J. Zhu, “Performance bounds of ranging precision in SPAD-based dToF LiDAR,” *Sensors*, vol. 25, no. 19, p. 6184, 2025.
- [65] J. W. Goodman, *Statistical Optics*, 2nd ed. John Wiley & Sons, 2015.
- [66] D. L. Snyder and M. I. Miller, *Random Point Processes in Time and Space*, 2nd ed. New York: Springer-Verlag, 1991.
- [67] G. Casella and R. Berger, *Statistical Inference*. Chapman and Hall/CRC, 2024.
- [68] D. Blackwell, “Conditional expectation and unbiased sequential estimation,” *The Annals of Mathematical Statistics*, pp. 105–110, 1947.
- [69] A. Ingle and D. Maier, “Count-free single-photon 3D imaging with race logic,” *IEEE Transactions on Pattern Analysis and Machine Intelligence*, vol. 47, no. 9, pp. 7292–7303, 2025.
- [70] I. Rech, A. Bovolenta, A. Cominelli, and G. Acconcia, “Toward constraintless time-correlated single-photon counting measurements: A new method to remove pile-up distortion,” *IEEE Journal of Selected Topics in Quantum Electronics*, vol. 30, no. 1, pp. 1–12, 2024.
- [71] G. Fratta, P. Daniele, I. Labanca, G. Acconcia, and I. Rech, “Near-zero distortion in TCSPC at more than one photon per excitation period: experimental validation,” *Optics Letters*, vol. 49, no. 17, pp. 4958–4961, 2024.
- [72] C. Meeks and P. Siegel, “Dead time correction via the time series,” *American Journal of Physics*, vol. 76, no. 6, pp. 589–590, 2008.
- [73] S. Usman and A. Patil, “Radiation detector deadtime and pile up: A review of the status of science,” *Nuclear Engineering and Technology*, vol. 50, no. 7, pp. 1006–1016, 2018.
- [74] D. Hampel and P. Lansky, “On the estimation of refractory period,” *Journal of Neuroscience Methods*, vol. 171, no. 2, pp. 288–295, 2008.
- [75] T. Akyurek, “A new dead-time determination method for gamma-ray detectors using attenuation law,” *Nuclear Engineering and Technology*, vol. 53, no. 12, pp. 4093–4097, 2021.
- [76] X. Qian, W. Jiang, A. Elsharabasy, and M. J. Deen, “Modeling for single-photon avalanche diodes: State-of-the-art and research challenges,” *Sensors*, vol. 23, no. 7, p. 3412, 2023.
- [77] J. Rapp, Y. Ma, R. M. A. Dawson, and V. K. Goyal, “High-flux single-photon lidar,” *Optica*, vol. 8, no. 1, pp. 30–39, 2021.
- [78] C. Zhang, S. Lindner, I. M. Antolović, J. Mata Pavia, M. Wolf, and E. Charbon, “A 30-frames/s, 252 × 144 SPAD flash LiDAR with 1728 dual-clock 48.8-ps TDCs, and pixel-wise integrated histogramming,”

- IEEE Journal of Solid-State Circuits*, vol. 54, no. 4, pp. 1137–1151, 2019.
- [79] S. W. Hutchings, N. Johnston, I. Gyongy, T. Al Abbas, N. A. Dutton, M. Tyler, S. Chan, J. Leach, and R. K. Henderson, “A reconfigurable 3D-stacked SPAD imager with in-pixel histogramming for flash lidar or high-speed time-of-flight imaging,” *IEEE Journal of Solid-State Circuits*, vol. 54, no. 11, pp. 2947–2956, 2019.
- [80] C. Zhang, N. Zhang, Z. Ma, L. Wang, Y. Qin, J. Jia, and K. Zang, “A 240×160 3D-stacked SPAD dToF image sensor with rolling shutter and in-pixel histogram for mobile devices,” *IEEE Open Journal of the Solid-State Circuits Society*, vol. 2, pp. 3–11, 2022.
- [81] O. Kumagai, J. Ohmachi, M. Matsumura, S. Yagi, K. Tayu, K. Amagawa, T. Matsukawa, O. Ozawa, D. Hirono, Y. Shinozuka *et al.*, “A 189×600 back-illuminated stacked SPAD direct time-of-flight depth sensor for automotive lidar systems,” in *2021 IEEE International Solid-State Circuits Conference (ISSCC)*, vol. 64. IEEE, 2021, pp. 110–112.
- [82] P. J. Bickel, C. A. J. Klaassen, Y. Ritov, and J. A. Wellner, *Efficient and Adaptive Estimation for Semiparametric Models*. Springer, 1993, vol. 4.
- [83] J. Rapp, Y. Ma, R. Dawson, and V. K. Goyal, “HighFluxSPL,” <https://github.com/Goyal-STIR-Group/HighFluxSPL>, 2021, MATLAB code for reproducing results from “High-flux single-photon lidar” (Optica, 2021).
- [84] C. H. Kraft and L. Le Cam, “A remark on the roots of the maximum likelihood equation,” *The Annals of Mathematical Statistics*, vol. 27, no. 4, pp. 1174–1177, 1956.
- [85] L. Le Cam, “On the asymptotic theory of estimation and testing hypotheses,” in *Proceedings of the Third Berkeley Symposium on Mathematical Statistics and Probability, Volume 1: Contributions to the Theory of Statistics*. University of California Press, 1956, pp. 129–156.
- [86] —, “Maximum likelihood: an introduction,” *International Statistical Review/Revue Internationale de Statistique*, pp. 153–171, 1990.
- [87] D. Shin, A. Kirmani, V. K. Goyal, and J. H. Shapiro, “Photon-efficient computational 3-d and reflectivity imaging with single-photon detectors,” *IEEE Transactions on Computational Imaging*, vol. 1, no. 2, pp. 112–125, 2015.
- [88] F. Heide, S. Diamond, D. B. Lindell, and G. Wetzstein, “Sub-picosecond photon-efficient 3D imaging using single-photon sensors,” *Scientific Reports*, vol. 8, no. 1, p. 17726, 2018.
- [89] D. F. Yu and J. A. Fessler, “Mean and variance of single photon counting with deadtime,” *Physics in Medicine & Biology*, vol. 45, no. 7, pp. 2043–2056, 2000.
- [90] J. Rapp and V. K. Goyal, “A few photons among many: Unmixing signal and noise for photon-efficient active imaging,” *IEEE Transactions on Computational Imaging*, vol. 3, no. 3, pp. 445–459, 2017.
- [91] S. Liu, X.-R. Yao, X.-F. Liu, D.-Z. Xu, X.-D. Wang, B. Liu, C. Wang, G.-J. Zhai, and Q. Zhao, “Pile-up effect in an infrared single-pixel compressive lidar system,” *Optics Express*, vol. 27, no. 16, pp. 22 138–22 146, 2019.
- [92] G. J. Kirchhoff, M. Hayman, W. J. Marais, J. P. Thayer, and R. A. Barton-Grimley, “Development of a photon-counting deadtime noise model that extends dynamic range and resolution in atmospheric lidar,” *Applied Optics*, vol. 64, no. 16, pp. 4568–4581, 2025.
- [93] T. H. Cormen, C. E. Leiserson, R. L. Rivest, and C. Stein, *Introduction to Algorithms*, 4th ed. MIT press, 2022.
- [94] F. Arvani and T. C. Carusone, “Direct time-of-flight TCSPC analytical modeling including dead-time effects,” in *2018 IEEE International Symposium on Circuits and Systems (ISCAS)*. IEEE, 2018, pp. 1–4.
- [95] A. Inconato, M. Locatelli, and F. Zappa, “Statistical modelling of SPADs for time-of-flight LiDAR,” *Sensors*, vol. 21, no. 13, p. 4481, 2021.
- [96] S. G. Johnson, “The NLOpt nonlinear-optimization package,” <https://github.com/stevengj/nlopt>, 2007.
- [97] D. C. Liu and J. Nocedal, “On the limited memory BFGS method for large scale optimization,” *Mathematical Programming*, vol. 45, pp. 503–528, 1989.
- [98] H. White, “Maximum likelihood estimation of misspecified models,” *Econometrica: Journal of the Econometric Society*, pp. 1–25, 1982.
- [99] Y. A. Kutoyants, *Statistical Inference for Spatial Poisson Processes*. Springer Science & Business Media, 2012, vol. 134.
- [100] I. M. Antolovic, S. Burri, C. Bruschini, R. Hoebe, and E. Charbon, “Nonuniformity analysis of a 65-kpixel CMOS SPAD imager,” *IEEE Transactions on Electron Devices*, vol. 63, no. 1, pp. 57–64, 2016.
- [101] S. P. Lalley, “The martingale central limit theorem,” <https://galton.uchicago.edu/~lalley/Courses/383/Lindeberg.pdf>, 2014, lecture notes, Dept. of Statistics, Univ. Chicago.